https://doi.org/10.5194/gmd-2020-303
Preprint. Discussion started: 20 January 2021

Geoscientific Model Development Discussions

TempestExtremes v2.1: A Community Framework for Feature Detection, Tracking and Analysis in Large Datasets

Paul A. Ullrich[1], Colin M. Zarzycki[2], Elizabeth E. McClenny[1], Marielle C. Pinheiro[1], Alyssa M. Stansfield[3], and Kevin A. Reed[3]

[1]Department of Land, Air and Water Resources, University of California, Davis, Davis, California
[2]Pennsylvania State University
[3]School of Marine and Atmospheric Sciences, State University of New York at Stony Brook, Stony Brook, New York

Correspondence: Paul Ullrich (paullrich@ucdavis.edu)

Abstract. TempestExtremes (TE) is a multifaceted framework for feature detection, tracking, and scientific analysis of regional or global Earth-system datasets on either structured and unstructured (native) grids. Version 2.1 of the TE framework now provides extensive support for examining both nodal and areal features, including tropical and extratropical cyclones, monsoonal lows and depressions, atmospheric rivers, atmospheric blocking, precipitation clusters, and heat waves. Available operations include nodal and areal thresholding, calculations of quantities related to nodal features such as accumulated cyclone energy and azimuthal wind profiles, filtering data based on the characteristics of nodal features, and stereographic compositing. This paper describes the core algorithms (kernels) that have been added to the TE framework since version 1.0, and gives several examples of how these kernels can be combined to produce composite algorithms for evaluating and understanding common atmospheric features and their underlying processes.

1 Introduction

For many atmospheric and oceanic features, automated object identification and tracking in large datasets has enabled targeted scientific exploration of feature-specific processes. Software tools for feature tracking, colloquially referred to as "trackers", are valuable for evaluating model performance (Davini and D'Andrea, 2016; Stansfield et al., 2020), understanding upstream process drivers (such as large-scale meteorological patterns; e.g., Grotjahn et al., 2016), and projecting future changes in feature characteristics and climatology (Roberts et al., 2020a). When well-engineered, these automated tools provide a means by which we can analyze the multiple petabytes of climate data now available (and anticipated in the next decade) (Schnase et al., 2016; Hassani et al., 2019). Since its introduction, TempestExtremes (TE, Ullrich and Zarzycki, 2017) has been continuously augmented with new kernels – that is, basic data operators that can act as building-blocks for more complicated tracking algorithms – designed to streamline data analysis and generalize capabilities present in other trackers. These kernels thus permit more options and flexibility in exploring the space of "valid" trackers for each feature, and enable a deeper understanding of how robust a given scientific conclusion is to the choice of tracker. Herein we describe the most significant of these updates and provide a number of use cases to demonstrate TE's functionality for real scientifically-driven case studies.

https://doi.org/10.5194/gmd-2020-303
Preprint. Discussion started: 20 January 2021

Geoscientific Model Development Discussions

Numerous publications over the past several decades have investigated automated algorithms for identification of both nodal and areal atmospheric features. Ullrich and Zarzycki (2017) Appendices A-C summarized dozens of such automated algorithms for extratropical cyclones, tropical cyclones, and tropical easterly waves. Even so, work to identify optimal tracking criteria continues (Murata et al., 2019). Beyond these traditionally tracked features, many recent papers have focused on defining regionally-relevant features such as monsoonal lows and depressions, associated with heavy precipitation in monsoonal regions (Hurley and Boos, 2015; Vishnu et al., 2020). Areal feature tracking algorithms have also been developed for clouds (Heikenfeld et al., 2019), atmospheric rivers (Shields et al., 2018; Rutz et al., 2019), atmospheric blocking (Scherrer et al., 2006), mesoscale convective systems (Prein et al., 2017; Feng et al., 2018), precipitation clusters (Clark et al., 2014; Pendergrass et al., 2016), and frontal systems (Hope et al., 2014; Schemm et al., 2015; Parfitt et al., 2017). Both nodal and areal algorithms generally feature a similar set of kernels, motivating the development of a single package encompassing relevant capabilities. For example, the majority of these algorithms are built upon an algorithmic paradigm known as MapReduce (Dean and Ghemawat, 2008), where individual timeslices are assessed independent of one another (an embarrassingly parallel "map" operation) then combined via a serial "reduce" operation. With significant commonality between these algorithms, there is clear value in bringing together this functionality under a single community-built and tested interface.

TE has been engineered with the goal of providing a comprehensive and user-friendly toolbox for feature tracking in model, reanalysis, or observational data products. It features many core design principles to enable its easy application in scientific analyses:

- The TE kernels are encapsulated in a variety of executables that are fully configurable from the command line (i.e. containing no hard-coded thresholds). Thus the processing operations performed by TE can be easily conveyed simply by communicating the relevant command line(s).
- TE abstracts many of the finer details about the structure of climate datasets through the use of physically-motivated kernels (such as the closed-contour operator), physically-based units, and internal indexing with CF-compliant time variables.
- TE directly addresses the need for high-throughput, readily usable, and standardized data analysis tools: namely, its kernels are individually implemented in optimized and, where appropriate, parallelized C++.
- TE also addresses a growing need for data analysis tools that work with "big data", enabling significant data volume reduction by isolating characteristics of individual features rather than total fields.
- TE is a fully open-source product, publicly developed and distributed via GitHub with permissive open source licensing.

These principles complement the underlying focii motivating TE's development, namely: robustness, usability, maintainability, and extensibility. To the best of the authors' knowledge, no other comprehensive toolkit exists for general nodal and areal feature tracking in climate datasets.

The remainder of this paper follows an analogous structure to Ullrich and Zarzycki (2017): Section 2 describes the core algorithms and kernels now available in TE version 2.1. In section 3, we present several examples of how these kernels can

https://doi.org/10.5194/gmd-2020-303
Preprint. Discussion started: 20 January 2021


Geoscientific Model Development Discussions

be combined together to form recipes for tracking tropical cyclones (TCs), for calculating fractional contribution of precipitation from TCs, for tracking and compositing extratropical cyclone fields, for tracking atmospheric rivers, and for tracking atmospheric blocks. A summary of results and future work is given in section 4.

2 TempestExtremes algorithms and kernels

In this section we describe the kernels available in the TE software package (organized by executable), with an emphasis on additions since TE version 1.0 – that is, essentially all of TE's executables and their core algorithms are described here except for DetectNodes and StitchNodes. Technical details on the operation of TempestExtremes can be found in the user guide (Ullrich, 2020). Notably, a key novelty of the functionality described here is its applicability to either unstructured or structured grids.

2.1 DetectNodes and StitchNodes

DetectNodes (formerly DetectCyclonesUnstructured) is used for the detection of nodal feature candidates, and corresponds to the parallel "map" step in the "MapReduce" framework – that is, candidate points are first downselected based on information at a single timeslice. DetectNodes is typically followed by StitchNodes, which represents the serial "reduce" operation in the chain; StitchNodes connects nodal features together in time and produces paths associated with singular features. Both of these executables and their algorithmic kernels are described in Ullrich and Zarzycki (2017), although version 2.1 now supports the use of physical time units for thresholds and time subsetting – e.g. `mintime` may be specified as a minimum number of timeslices (e.g. `"5"`) or as the minmum number of hours between first and last candidate in a path (e.g. `"24h"`).

2.2 NodeFileEditor

NodeFileEditor is a new addition to TE that encapsulates functionality for editing of nodefiles (outputs from DetectNodes) through the calculation of auxiliary quantities or filtering of existing quantities. A list of functions currently available in NodeFileEditor are given in Table 1. These functions may be chained to perform multiple related operations, such as computing a radial wind profile of a tropical cyclone and then extracting the radius where a particular wind threshold is exceeded. An example of such chaining of commands is given in section 3.3.

Most of the implemented algorithms are straightforward except for `max_closed_contour`, whose pseudocode is provided in Algorithm 1. Intuitively, this algorithm can be thought of as filling up a 3D extruded surface representative of the contours of the field until fluid spills farther out than the prescribed maximum distance. The last height difference is then recorded as the maximum delta for the closed contour.

2.3 NodeFileFilter

NodeFileFilter encapsulates algorithms for filtering spatial data using nodefile information – effectively converting nodefiles into binary raster masks at each timeslice and (optionally) applying them to available data. Filtering can be performed using

https://doi.org/10.5194/gmd-2020-303
Preprint. Discussion started: 20 January 2021

Geoscientific Model Development Discussions

Operator	Description
eval_ace	Calculate the instantaneous accumulated cyclone energy (ACE, Bell et al. (2000)), equal to $10^{-4} u_{kt,max}^2$ where $u_{kt,max}$ is the maximum wind speed within a prescribed radius of the nodal feature, in knots. We use a value of 1.94384 kt (m s^{-1})$^{-1}$ to convert m s^{-1} to kt.
eval_acepsl	Approximate ACE using sea level pressure to predict surface wind speed (ACEPSL). Currently ACEPSL is calculated as ACE, but using $u_{kt,max} = 1.94384$ kt (m s^{-1})$^{-1} \times 3.92 \times (1016.0 \text{ hPa} - psl_{min})^{0.644}$ (Holland, 2008), where psl_{min} is the minimum sea level pressure within a prescribed radius.
eval_ike	Calculate that instantaneous integrated kinetic energy (Powell and Reinhold, 2007), defined as $\sum_i \frac{1}{2} u_i^2 A_i$, where the sum is taken over all grid cells within a prescribed radius, u_i is the magnitude of the wind speed at that grid cell (in m s^{-1}), and A_i is the area of that grid cell in m^2.
eval_pdi	Calculate the power dissipation index (Emanuel, 2005), defined as u_{max}^3, where u_{max} is the maximum wind speed within a prescribed radius in m s^{-1}.
radial_profile	Develop a radial profile of the specified variable at each timeslice around the nodal feature point by binning and averaging gridpoint values. The output is expressed as a python-format array.
radial_wind_profile	As radial_profile but for the radial and azimuthal wind speed. The radial and azimuthal components are computed by projecting the 2D velocity at each grid point onto the radial and azimuthal vector fields around each nodal feature prior to binning.
lastwhere	Given an array as input (such as the output of radial_profile) identify the last element of the array that satisfies a given threshold (e.g. used for determining the radius at which azimuthal wind speed is greater than 8 m s^{-1}).
value	Given an array extract the value at the specified index using linear interpolation.
max_closed_contour	For a given field determine the largest value that could be used to satisfy the closed contour criteria (see Ullrich and Zarzycki (2017) section 2.6) around each nodal feature (see Algorithm 1).
region_name	Given containing the names and coordinates of polygons in longitude-latitude space, identify the name of the region for a given pointwise feature. Each point is identified as being in a given region using a straight-line test along lines of constant latitude – if the number of intersections with edges of the polygon is odd (even) then the point is inside (outside).

Table 1. Functions implemented in NodeFileEditor as of TempestExtremes version 2.1.

https://doi.org/10.5194/gmd-2020-303
Preprint. Discussion started: 20 January 2021

Geoscientific Model Development Discussions

Algorithm 1 Determine the maximum closed contour delta (largest field delta that permits a closed contour within the given distance of the feature) for each node in a given nodefile `N`, over field `F` and maximum distance `maxdist`. This algorithm uses a priority queue, which places the node with the highest priority (in this case the smallest delta) at the top of the queue.

```
max_delta = max_closed_contour(nodefile N, field F, maxdist)

  for each node n in N
    max_delta[n] = 0
    define empty priority_queue pqueue
    insert node n into pqueue with delta 0
    visited = []
    while pq is not empty
      p = remove node from pqueue with lowest delta
      add p to visited
      for all neighbors q of p
        if q is not in visited then add q to pqueue with delta (F[q] - F[n])
      if (dist(p,n) < maxdist) and (F[p] - F[n] > max_delta[n]) then
        max_delta[n] = F[p] - F[n]
```

the distance from each feature, based on the closed contour of each feature (as described by Algorithm 2), or by thresholding of areal regions that are within a given distance of each nodal feature (as described by Algorithm 3). The latter is useful for identifying, for instance, precipitation clusters associated with tropical cyclones.

2.4 NodeFileCompose

NodeFileCompose encapsulates functionality for taking snapshots of fields (i.e., storm extraction) or compositing fields either around a nodal feature or over a particular geographic region. Most commonly this is used for constructing compositions on the stereographic plane centered on each feature. Such stereographic composites are computed using Algorithm 4. The mathematical operators used for the local stereographic projection are given in Appendix A.

2.5 DetectBlobs

DetectBlobs is used for identifying areal features (blobs), such as atmospheric blocks, atmospheric rivers, or precipitation clusters. As with DetectNodes, this executable represents the parallel "map" step in the "MapReduce" framework. Candidate regions are selected based on information at a single timeslice, typically simple thresholds such as "all points where precipita-

https://doi.org/10.5194/gmd-2020-303
Preprint. Discussion started: 20 January 2021

Geoscientific Model Development Discussions

Algorithm 2 Generate a binary mask using the closed contour criteria, given nodefile `N`, field `F`, closed contour magnitude `delta`, maximum mask distance `dist`, and maximum distance for minima/maxima search `minmaxdist`. The functions `find_min_near` and `find_max_near` are given by Algorithm 4 in Ullrich and Zarzycki (2017).

```
M = mask_by_closed_contour(nodefile N, field F, delta, dist, minmaxdist)

  for each node n in N
    if (delta > 0) m = find_min_near(n, F, minmaxdist)
    if (delta < 0) m = find_max_near(n, F, minmaxdist)
    visited = []
    tovisit = [m]
    ref_value = F[m]
    while tovisit is not empty
      p = remove node from tovisit
      if visited contains p then continue
      add p to visited
      if (dist(p,m) > dist) then continue
      if (sign(delta) * (F[p] - F[m]) > abs(delta)) then continue
      M[p] = 1
      add neighbors of p to tovisit
```

tion is greater than 1 mm day^{-1}". Features are marked using a binary mask and output stored in NetCDF format. Contiguous regions may then be excluded based on either geometric thresholds or using criteria derived from other variables. DetectBlobs supports MPI-based parallelism.

2.6 StitchBlobs

StitchBlobs is used for tracking areal features (blobs) in time, assigning connected features a unique global id and/or applying time-dependent criteria to each contiguous region. Given input as a time-dependent binary mask variable, blobs that overlap in sequential time steps will be assigned the same global identifier. The algorithm implemented in TE for connecting blobs in time uses a forward-backward search that can treat the 2D space + 1D time object as a single object, allowing for both splitting and recombining of features in time.

The pseudocode for this search protocol is provided in Algorithms 5 and 6, and its operation illustrated in Figure 1. Put briefly, contiguous regions at each timeslice are identified using a flood fill algorithm and assigned a unique tag of the form (time id, blob id). An additional "merge distance" argument can be specified that merges nearby blobs at each timeslice if their

https://doi.org/10.5194/gmd-2020-303
Preprint. Discussion started: 20 January 2021

Geoscientific Model Development Discussions

Algorithm 3 Generate a binary mask by picking out blobs satisfying a threshold within a given radius of each node. The inputs include the nodefile `N`, field `F`, the search distance `searchdist`, threshold operation `threshold`, and maximum mask distance `maxdist`.

```
M = mask_by_nearbyblobs(nodefile N, field F, searchdist, threshold, maxdist)

  for each node n in N
    visited = []
    tovisit = [n]
    while tovisit is not empty
      p = remove node from tovisit
      if visited contains p then continue
      add p to visited
      if (dist(p,n) > searchdist) then continue
      add neighbors of p to tovisit

      if F[p] does not satisfy threshold then continue
      tovisitnested = [p]
      while tovisitnested is not empty
        q = remove node from tovisitnested
        if visited contains q then continue
        add q to tovisitnested
        if (dist(q,n) > maxdist) then continue
        if F[q] does not satisfy threshold then continue
        M[q] = 1
        add neighbors of q to tovisitnested
```

https://doi.org/10.5194/gmd-2020-303
Preprint. Discussion started: 20 January 2021

Geoscientific Model Development Discussions

Algorithm 4 Generate a stereographic composite of field `F` over the given set of nodes `N`, generated by DetectNodes. The stereographic grid has resolution `res` and grid spacing `dist`, given as the great circle distance along coordinate lines passing through the origin.

```
field C = stereographic_composite(field F, node_list N, res, dist)
  C = empty 2D stereographic grid with parameters (res,dist)
  for each node n in N
    G = generate 2D stereographic grid with parameters (res,dist) centered on n
    for each node m in G
      use inverse stereographic projection to obtain point p corresponding to G[m]
      q = nearest grid point in F to p
      assign G[m] to value F[q]
    C = C + G
  C = C / size(N)
```

perimeters are within this specified distance. A graph is then constructed with each of these tags corresponding to the nodes of the graph. Edges are then added to the graph where two sequential areal features are deemed to be connected in time. Finally, the components of the graph are assigned a unique global id, with lower global ids corresponding to blobs that first appear at earlier times.

By default, areal features are deemed to be connected in time if they share at least one grid point at sequential times (regardless of the area of that grid point). For example, in Figure 1, areal regions (1,1) and (2,1) overlap in space and so are deemed to be connected. If a stricter threshold on the overlap area is needed for blobs at sequential timeslices to be deemed part of the same cluster, StitchBlobs provides arguments `min_overlap_prev`, `max_overlap_prev`, `min_overlap_next`, `max_overlap_next`. The values specified by these arguments are percentages based on the area of the feature at each timeslice. The `min_*` arguments specify minimum overlap area and `max_*` specify maximum overlap area. The `*_prev` arguments use the blob at the past timeslice as reference, whereas `*_next` uses the blob at the future timeslice. In this example, blob tag (2,2) has a 25% overlap with blob tag (1,2); thus these two blobs are only deemed to be connected if the value 25 is within the range specified by `[min_overlap_prev, max_overlap_prev]`. Similarly blob tag (2,1) has a 50% overlap with blob tag (2,2); thus these two blobs will be connected if the value 50 is within the range specified by `[min_overlap_next, max_overlap_next]`.

https://doi.org/10.5194/gmd-2020-303
Preprint. Discussion started: 20 January 2021

Geoscientific Model Development Discussions

Algorithm 5 Flood fill blobs on unstructured grid using breadth-first graph search over binary field `G`, merging blobs within the given distance `merge_dist`.

```
blob set array S =
  flood_fill_and_tag_with_merging(binary_field G, merge_dist)

  % Perform flood fill and tag
  current_tag = 0
  visited = []
  kdP = empty array of kdtrees
  P = array storing perimeter points for each tag
  for each node p
    if (F[p] is not 0) and (visited does not contain p) then
      current_tag = current_tag + 1
      tovisit = [p]
      while tovisit is not empty
        q = remove node from tovisit
        if visited contains q then continue
        add q to visited
        if (F[q] is not zero) then
          insert q into S[current_tag]
          add neighbors of q to tovisit
          if any neighbors r of q have (F[r] = 0) then
            add q to P[current_tag] and kdP[current_tag]

  % Build list of blobs to merge by distance
  M = empty graph with integer nodes denoting merged blobs
  for all ordered pairs of tags (s,t)
    for all nodes p in P[s]
      if nearest neighbor from kdP[t] is closer than merge_dist then
        add edge (s,t) to M

  % Merge blob sets
  for each tag t from 1 to current_tag
    find minimum tag s of connected subgraph containing t
    merge S[t] into S[s]
```

https://doi.org/10.5194/gmd-2020-303
Preprint. Discussion started: 20 January 2021

Geoscientific Model Development Discussions

Algorithm 6 Forward-backward algorithm for areal-feature search. Given a time series of binary fields `G[t]`, a merge distance `merge_dist` and overlap thresholds `min_overlap_*` and `max_overlap_*`.

```
field F[t] = stitch_blobs(binary_field G[t], merge_dist,
  min_overlap_prev, max_overlap_prev,
  min_overlap_next, max_overlap_next)

  % Use flood fill and merge to identify blobs
  for all times t from 0 to length(G)
    S[t] = flood_fill_and_tag_with_merging(G[t], merge_dist)

  % Build overlap graph
  M = empty graph denoting (time,blob) pairs
  for all times t from 0 to length(G)
    for all blobs p in S[t]
      insert node (t,p) into M

  % Identify blobs to be stitched together in time
  for all times t from 0 to length(G)-1
    for all blobs p in S[t]
      for all blob n in S[t+1]
        prev_area = area of S[t][p]
        next_area = area of S[t+1][n]
        overlap_area = overlap area between S[t][p] and S[t+1][n]
        if (overlap_area / prev_area >= min_overlap_prev) then
          and (overlap_area / prev_area <= max_overlap_prev)
          and (overlap_area / next_area >= min_overlap_next)
          and (overlap_area / next_area <= max_overlap_next)
            add edge ((t,p),(t+1,n)) to M
    S_prev = S_next

  % Assign a common global_id to overlapping blobs
  global_id = 1
  for all nodes (t,p) in M
    for each node (tx,px) in connected subgraph of M containing (t,p)
      for each node p in S[tx][px]
        F[t][p] = global_id
    global_id = global_id + 1
```

https://doi.org/10.5194/gmd-2020-303
Preprint. Discussion started: 20 January 2021

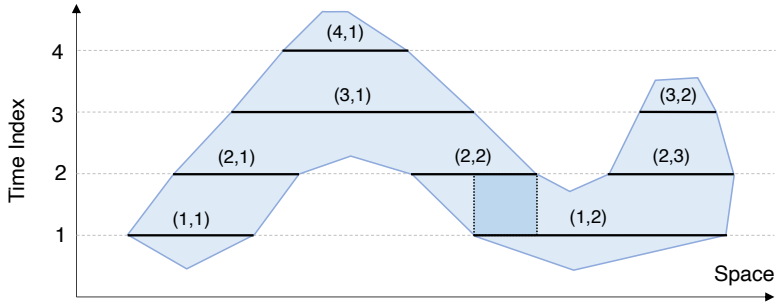

Figure 1. A depiction of Algorithms 5 and 6 for forward-backward areal feature search used by StitchBlobs, simplified to show one space dimension (e.g. longitude) and the time dimension.

2.7 Other Utilities

In addition to the "core" functionality described in previous sections, TE also provides a number of other utilities to manage nodefiles, blobfiles, and other climatological data relevant to feature tracking. These are briefly mentioned here as this functionality is employed in the composite tracking algorithms and analysis of section 3.

- *Climatology* is used for constructing climatological time series, including long-term daily, monthly, seasonal, and annual means. It supports parallel execution via MPI, as well as arguments that can be used to limit the amount of memory used by each thread.
- *FourierFilter* is used for Fourier filtering/smoothing of input data series. Although it provides a general implementation that could be used for any dataset, it has primarily been used for smoothing long-term daily means produced from Climatology.
- *VariableProcessor* provides direct access to TE's internal variable processing capability, allowing arithmetic and grid-based operations to be applied to gridded data files. The operation of this utility is roughly analogous to that of the NetCDF Operator (NCO, Zender (2008)) `ncap2`.

3 Selected examples

In this section we present selected examples of tracking and analysis of different features – that is, different recipes for combining the algorithmic kernels described in section 2 to produce composite tracking and analysis algorithms. In all examples, the corresponding TE command lines are provided to both demonstrate that these command lines are effective at conveying the operation in a human-readable manner and to enable reproducibility of our results. Past examples from the literature using TE are provided in section 3.1. This is then followed by a several examples of composite tracking algorithms assembled using TE's tracking kernels, and subsequent employ of TE for characterization and analysis. These examples include TC tracking in ERA5, fractional contribution of precipitation from TCs in ERA5 and TRMM, atmospheric river tracking, extratropical

https://doi.org/10.5194/gmd-2020-303
Preprint. Discussion started: 20 January 2021


Geoscientific Model Development Discussions

cyclone tracking in CMIP6 data, and finally generation of an atmospheric blocking climatology using MERRA2 data. In each step of these composite algorithms we provide the actual TE command lines as they are effective at conveying, in a manner easily understood by a human reader, the tunings employed in configuring each algorithm.

3.1 Examples from the existing literature

Since version 1.0, TE has been employed for feature tracking in a number of scientific studies. Here we catalogue known publications emerging from those studies, organized by feature type:

Tropical Cyclones (TCs): More than any other feature, TE has been employed for the study of TCs. The TC tracker was first used to understand intensity errors associated with one-way coupling between ocean and atmosphere in Zarzycki (2016). It was subsequently used to investigate the TC wind-pressure relationship in Chavas et al. (2017), a relationship later revisited in Moon et al. (2020) where TE was used to assess its sensitivity to model resolution. In Wing et al. (2019), TE was applied to native grid data produced using the Community Atmosphere Model Spectral Element (CAM-SE) dynamical core to track TCs; outputs were then used to investigate the processes underlying moist intensification of TCs. A related study by Camargo et al. (2020) used this dataset to investigate the large-scale environment around TCs. In Roberts et al. (2020a) and Roberts et al. (2020b), TE-derived TC tracks were used to understand resolution sensitivity and future change in both historical and future HighResMIP experiments (Haarsma et al., 2016) across several models. Along these lines, Balaguru et al. (2020) used TE to characterize TC climatology in the Energy Exascale Earth System Model (E3SM). Reed et al. (2020) used TE to extract tracks of Hurricane Florence and attribute human influence on this storm. TE has also been used for tracking storms in aquaplanet simulations (Chavas and Reed, 2019) to better understand how thermal forcing impacts TC genesis and size. Recent work by Stansfield et al. (2020) has also leveraged some of the more advanced capabilities in TE to filter fields (e.g., precipitation) in the vicinity of tracked features to evaluate model performance.

Extratropical Cyclones (ETCs): In order to better understand cyclonic storms and their impacts, Zarzycki et al. (2017) developed the ExTraTrack software framework atop TE to track TCs and ETCs through their entire lifecycle. This module enabled cyclonic storms to be examined using the thermal wind and thermal asymmetry phase space of Hart (2003). ExTraTrack was later applied to a suite of high-resolution global simulations in Michaelis and Lackmann (2019). ETCs were also tracked in the Community Earth System Model Large Ensemble (CESM-LENS) in Zarzycki (2018) to understand the drivers responsible for snowstorms in the US Northeast. Then in Small et al. (2019), extratopical storms tracked using TE were used to determine if resolution of ocean fronts improves the representation of simulated storm tracks. In Zhang et al. (2020) the vertical symmetry criteria from ExTraTrack was also adapted for tracking of Mediterranean Hurricanes (Medicanes). Finally, TE was also used to track ETCs as part of an effort to evaluate severe local storm environments in climate models and reanalysis (Li et al., 2020).

Monsoonal lows and depressions: Analogous to the study of Zarzycki and Ullrich (2017), Vishnu et al. (2020) optimized DetectNodes for tracking of monsoon lows and depressions. A comprehensive analysis of input fields found that 850hPa streamfunction tended to produce better results compared with trackers based on sea level pressure, vorticity, and geopotential. A weighted Critical Success Index (CSI) (Di Luca et al., 2015) was used to determine tracker performance. However, acknowledging the possibility of errors in the reference dataset (here the Sikka archive), the weighted CSI index used in this analysis

https://doi.org/10.5194/gmd-2020-303
Preprint. Discussion started: 20 January 2021


Geoscientific Model Development Discussions

also considered the degree to which a track is represented similarly across all reanalyses. A related study by Zhang et al. (2019) also tracked tropical depressions in the North Indian Ocean in 2018 to investigate anthropogenic impact on this storm season.

Atmospheric blocking: In Pinheiro et al. (2019), a suite of atmospheric blocking methods from TE were applied to ERA-Interim data to better understand sensitivities of atmospheric blocks to the detection algorithm and the meteorological environment around blocking features.

Atmospheric rivers (ARs): Atmospheric river tracking with TE was first documented as part of the Atmospheric River Transport Method Intercomparison Project (ARTMIP) in Shields et al. (2018), and later in Rutz et al. (2019). The proposed algorithm used the Laplacian of the integrated vapor transport (IVT) field rather than the IVT field itself, thus flagging IVT "ridges" rather than IVT over a threshold. This choice was made to address with issues of stationarity generally present in trackers using an IVT threshold. TE's algorithm has since been used both for AR detection and tracking (with DetectBlobs and StitchBlobs) in Rhoades et al. (2020b), Rhoades et al. (2020a), Patricola et al. (2020), and McClenny et al. (2020).

3.2 Tropical Cyclone Tracking in ERA5

In Zarzycki and Ullrich (2017), a sensitivity analysis was applied to optimize DetectNodes for the detection of tropical cyclones by benchmarking hit rate (HR) and false alarm rate (FAR) from reanalysis products against the International Best Track Archive for Climate Stewardship (IBTrACS; Knapp et al., 2010). The resulting configuration, which tracked storms based on sea level pressure minima, produced the highest HR minus FAR differential in the literature across a wide range of reanalysis products. An interesting result that emerged from this analysis was that upper level geopotential layer thickness (typically Z300 minus Z500) was the most robust indicator of an upper level warm core across products. In this section we apply the same configuration that provided maximal agreement between earlier-generation reanalyses and IBTrACS to ERA5 input (Hersbach et al., 2020) so as to identify ERA5 TC tracks.

3.2.1 Step 1: DetectNodes

The first step in the TC tracking process is the detection of TC candidates, which are points that have both a sea-level pressure minima and an upper level warm core. These conditions are codified via the following command line:

```
DetectNodes --in_data_list ERA5_TC_files.txt --timefilter "6hr"
  --out_file_list ERA5_DN_files.txt
  --searchbymin MSL
  --closedcontourcmd "MSL,200.0,5.5,0;_DIFF(Z(300hPa),Z(500hPa)),-58.8,6.5,1.0"
  --mergedist 6.0
  --outputcmd "MSL,min,0;_VECMAG(VAR_10U,VAR_10V),max,2;ZS,min,0"
```

For this example, our ERA5 data is comes from the NCAR Research Data Archive (European Centre for Medium-Range Weather Forecasts, 2019), with 3D time-series data provided at hourly resolution in daily chunks, 2D time-series data provided at hourly resolution in monthly chunks, and 2D invariant data provided in a single file. The `timefilter` argument here indi-

https://doi.org/10.5194/gmd-2020-303
Preprint. Discussion started: 20 January 2021


Geoscientific Model Development Discussions

cates that data should be downselected to six-hourly, which is typical for analysis of TCs. As different variables are distributed across multiple files, the first two lines of the input data consist of several files containing 3D geopotential height on pressure surfaces (Z), 2D mean sea level pressure (MSL), 2D 10 meter zonal and meridional wind speeds (VAR_10U and VAR_10V), and surface elevation (ZS), stringed together by semicolons. Note that TE supports different agglomerations of timeslices, as it uses the CF-compliant time to match timeslices across files.

To first limit the search space of possible TCs, we identify candidates as local minima in the sea level pressure field. Two closed contour criteria are used to eliminate candidates. As argued in Ullrich and Zarzycki (2017), the closed contour criteria is desirable since it mitigates some of the effects that arise on unstructured grids and makes the criteria more robust across resolutions. The first criteria is `"MSL,200.0,5.5,0"`, which indicates that MSL must increase by 200 (Pa) over a distance of 5.5° great-circle-distance (GCD) from the candidate point (the low pressure region must be of sufficient magnitude and sufficiently compact to be considered coherent). The second criteria is `"_DIFF(Z(300hPa),Z(500hPa)),-58.8,6.5,1.0"` which indicates that the difference between geopotential (Z) on the 300hPa and 500hPa surfaces must decrease by 58.8 m^2 s^{-2} (equal to 6 m geopotential height) over a distance of 6.5° GCD, using the maximum value of this field within 1° GCD as reference. This second criteria indicates that there must be a coherent upper-level warm core attached to the local low so as to structurally differentiate these features from extratropical systems. This further provides an example of the ability of TE to evaluate functional relationships at run-time. Finally, candidates that have been identified with this protocol are eliminated if a stronger minima exists within 6 degrees great circle distance.

The remaining `outputcmd` argument indicates three additional outputs that are calculated and output as additional columns in each nodefile. Here `"MSL,min,0"` outputs the value of MSL at the candidate point, `"_VECMAG(VAR_10U,VAR_10V),max,2"` outputs the maximum magnitude of the vector wind at 10 m altitude within 2° GCD of the candidate, and `"ZS,min,0"` outputs the surface height at the candidate point. These variables are needed in the subsequent StitchNodes step to construct and filter TC trajectories.

3.2.2 Step 2: StitchNodes

The next step is to concatenate nodefiles and perform feature tracking (the "Reduce" operation in the MapReduce framework). Tracks are formed using the StitchNodes command, as follows:

```
StitchNodes  --in_list ERA5_DN_files.txt --out ERA5_TC_tracks.txt
  --in_fmt "lon,lat,slp,wind,zs"
  --range 8.0 --mintime "54h" --maxgap "24h"
  --threshold "wind,>=,10.0,10;lat,<=,50.0,10;lat,>=,-50.0,10;zs,<=,150.0,10"
```

The first three arguments here indicate the input candidate nodefile (produced by DetectNodes) and the output nodefile. The format of these files differ because they convey different information – the former conveying candidates detected at each time slice, and the latter containing paths, or lists of candidates from different time slices. Nonetheless auxiliary candidate information computed with DetectNodes' `outputcmd` is preserved.

https://doi.org/10.5194/gmd-2020-303
Preprint. Discussion started: 20 January 2021


Geoscientific Model Development Discussions

The relevant tuning parameters are specified by `range`, `mintime` and `maxgap` and refer to the maximum distance (in degrees GCD) that a feature can move between subsequent detections, the minimum persistence time of each trajectory (calculated as the time between initiation and termination), and the maximum duration between two sequential detections, respectively. In particular, `maxgap` is a novel option that allows for a path to be missing candidates for some timeslices (for instance due to temporary weakening of TC as it passes over land).

Four field-dependent thresholds are then specified for a trajectory to be accepted. The first threshold `"wind,>=,10.0,10"` indicates that the wind magnitude (derived from the "wind" column in the nodefile) must be greater than 10 m s^{-1} for at least 10 timeslices; this ensures that these features are sufficiently intense to be classified as tropical storms. The next two thresholds `"lat,<=,50.0,10;lat,>=,-50.0,10"` indicate that the latitude of the feature must be between 50S and 50N for at least 10 timeslices, so as to eliminate any extratropical features that could not have existed as tropical storms. The final threshold `"zs,<=,150.0,10"` indicates that the feature must exist at an elevation below 150 m for at least 10 timeslices; this removes false alarms that can often appear in regions of rough topography associated with PSL correction formulations.

3.2.3 Tropical cyclone trajectories

Figure 2 depicts the tropical cyclone trajectories produced from this analysis in ERA5. Storms are color-coded by sea level pressure as opposed to surface winds since it has been found that the former is better resolved in coarser datasets (Chavas et al., 2017), although this may overestimate storm intensity at higher latitudes where storms are beginning to undergo extratropical transition. While storms are generally too weak in aggregate, a common problem amongst reanalyses (Schenkel and Hart, 2012; Murakami, 2014; Hodges et al., 2017), the method shows high spatial and temporal correlation of storm climatology when compared to observational products such as IBTrACS, and produces superior hit rates (78% for all TCs and 95% for those with wind speeds exceeding 33 m s^{-1}) and false alarm ratios (14% globally) when compared to many legacy tracking techniques (Zarzycki et al., revised).

3.3 Fractional contribution of precipitation from TCs

As argued by Schenkel et al. (2017), the largest radius outside of the eyewall where the azimuthally-averaged wind speed exceeds 8 m s^{-1} (r8) tends to be a good measure of the outer size of a TC. In Stansfield et al. (2020), TE was used to examine the distribution of r8 among TCs in reanalysis data in ERA5 and a series of runs from the Community Earth System Model (CESM). This paper further compared and contrasted TC-related precipitation within r8 against precipitation within a fixed distance of 500 km.

For the examples here, we calculate the fractional contribution of precipitation from TCs for one reanalysis dataset, ERA5, and one observational dataset, the Tropical Rainfall Measuring Mission (TRMM3B42; Huffman et al., 2007). For ERA5, the TC track files are created as described in Section 3.2. For TRMM, the IBTrACS dataset is used for TC track observations. Because there are limited comprehensive and long-term observational datasets of complete TC wind fields, ERA5 wind field data is combined with IBTrACS to calculate the outer radius, r8, at every timestep for all historical TC tracks for the TRMM analysis.

https://doi.org/10.5194/gmd-2020-303
Preprint. Discussion started: 20 January 2021

Geoscientific Model Development Discussions

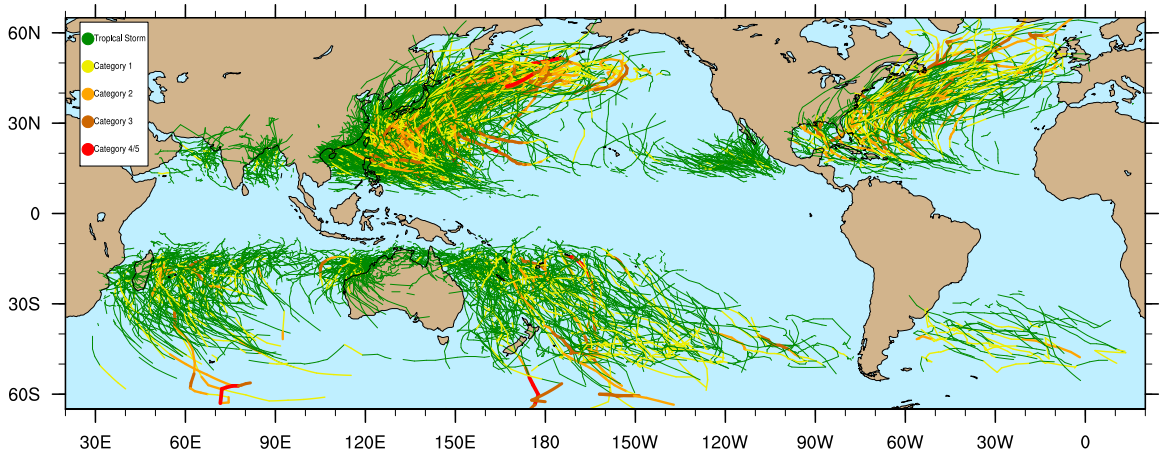

Figure 2. Tropical cyclone trajectories from ERA5 over the period 1980-2019, inclusive. Coloring denotes the instantaneous Saffir-Simpson category of the tropical cyclone as measured by sea level pressure and applying the pressure-wind relationship of Atkinson and Holliday (1977) with updated coefficients from Knaff and Zehr (2007).

3.3.1 Step 1: NodeFileEditor

To begin, radial profiles and radius of 8 m s^{-1} wind are added to the nodefile generated in section 3.2.2 and the IBTrACS nodefile (not shown):

```
NodeFileEditor --in_data_list ERA5_TC_files.txt --in_nodefile ERA5_TC_tracks.txt
  --in_fmt "lon,lat,slp,wind,zs" --out_nodefile ERA5_TC_radprofs.txt
  --out_fmt "lon,lat,rsize,rprof" --time_filter "6hr"
  --calculate "rprof=radial_wind_profile(VAR_10U,VAR_10V,159,0.125);
  rsize=lastwhere(rprof,>,8)"
```

The input to this operation includes the files containing the 2D ERA5 10 meter zonal and meridional wind speeds (VAR_10U and VAR_10V), and the nodefile generated in section 3.2.2. As part of this analysis we also augment an IBTrACS nodefile in a similar manner, using the IBTrACS TC tracks, but ERA5 winds to estimate TC size (command line not shown here). As in section 3.2.1, a time filter is used to only analyze 6-hourly time slices of data. Internal to the execution of this command is the construction of a date object for each entry of the nodefile, which is then cross-referenced against every timeslice in the list of datafiles to find the corresponding field – in this way indexing is abstracted from the user.

The calculations requested from NodeFileEditor are specified by the `calculate` argument, executed from left to right. First the radial profile is computed with `radial_wind_profile(VAR_10U,VAR_10V,159,0.125)` and stored in variable `rprof`. These arguments indicate which variables should be used for the calculation, and that the radial profile should consider of 159 bins of width 0.125 degrees GCD. After the radial profile is calculated, the last value where the radial wind

https://doi.org/10.5194/gmd-2020-303
Preprint. Discussion started: 20 January 2021


Geoscientific Model Development Discussions

profile is greater than 8 m s^{-1} is located and output to the nodefile. The last value in the array is taken because we want to avoid recording the radius of the 8 m s^{-1} wind within the TC inner core.

3.3.2 Step 2: NodeFileFilter

Once the nodefile has been updated, the 8 m s^{-1} radius is then employed to build a circular mask around each tracked object:

```
NodeFileFilter --in_nodefile ERA5_TC_radprofs.txt --in_fmt "lon,lat,rsize,rprof"
  --in_data_list ERA5_precip_files.txt --out_data_list ERA5_filtered_precip_files.txt
  --var "PRECT" --bydist "rsize"
```

The input nodefile is the output nodefile from NodeFileEditor, now augmented with the radius of 8 m s^{-1} winds. The input data contain 6-hourly ERA5 precipitation data from the NCAR Research Data Archive (European Centre for Medium-Range Weather Forecasts, 2019) under variable name `PRECT`. Precipitation in ERA5 is calculated from hourly forecasts initialized from the analysis at 06:00UTC and 18:00UTC. Precipitation is converted from hourly to 6-hourly by adding up the accumulated precipitation 3 hours before and 3 hours after the desired timesteps of 00:00UTC, 06:00UTC, 12:00UTC, and 18:00UTC. For example, to calculate 6-hourly precipitation at 06:00UTC, the precipitation from 03:00UTC to 09:00UTC is added up. For the TRMM analysis, the TRMM precipitation data is originally 3-hourly, so before analysis the TRMM data is summed into 6-hourly data. This is done using a centered averaging method, so for example, to calculate 6-hourly precipitation at 06:00UTC, half of the 03:00UTC precipitation, all of the 06:00UTC precipitation, and half of the 09:00UTC precipitation are added up. Output consists of a sequence of NetCDF files, one for each input file, containing filtered precipitation.

The final argument specifies how the filtering is performed, in this case "by distance" using `rsize`. This procedure only keeps precipitation grid point values that are within this distance of each detected TC. Internally to NodeFileFilter, the mask is computed through the employ of a kd-tree (see discussion in Ullrich and Zarzycki (2017)).

3.3.3 TC Precipitation Climatology

Figure 3 shows the percent contribution to global precipitation from TCs for ERA5 and TRMM, calculated by using NCO's `ncra` to sum up the TC precipitation within r8 filtered by NodeFileFilter and dividing it by the sum of the total precipitation over the entire length of the datasets (1985-2019 for ERA5 and 1998-2014 for TRMM). The areas of largest TC contribution align with the areas of the highest TC activity shown in Figure 2 and typically occur over the ocean, in broad agreement with Prat and Nelson (2013). Khouakhi et al. (2017) (their Figure 3b) made a similar plot, except using land-based gauge data and for a slightly different time period, and showed similar locations of maximum contributions of 40-50% over northwestern Australia and eastern Asia.

3.4 Extratropical cyclones

Extratropical cyclones (ETCs) are mid-latitude, synoptic scale weather features responsible for a host of impacts, including high winds, coastal surge, and heavy precipitation, which can fall as rain, snow, sleet, or freezing rain (Schultz et al., 2019;

https://doi.org/10.5194/gmd-2020-303
Preprint. Discussion started: 20 January 2021

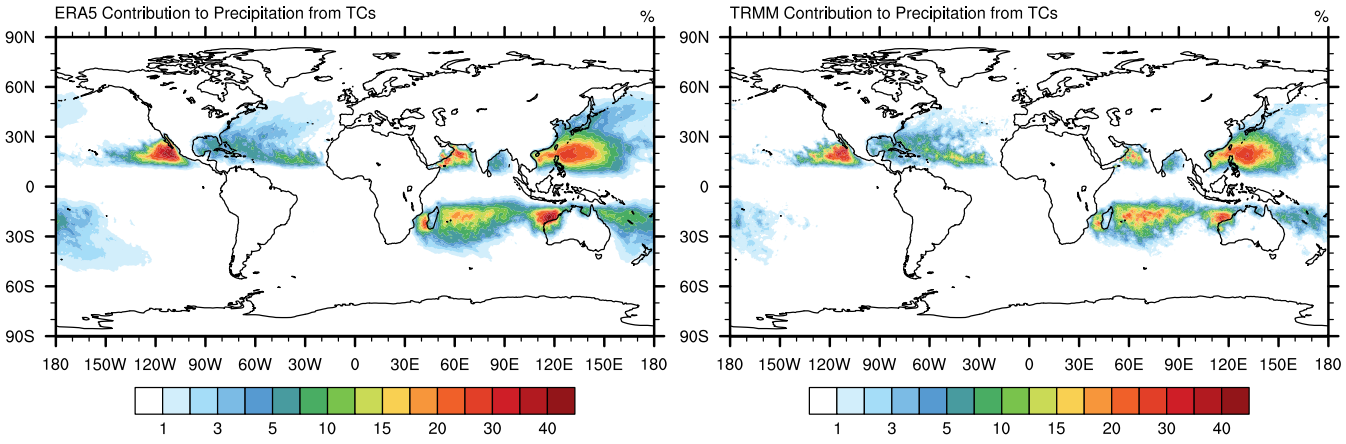

Figure 3. Percent contribution to precipitation from tropical cyclones using precipitation field from (left) ERA5 and (right) TRMM.

Dacre, 2020). Even though these features occur at relatively large spatial scales, models still have difficulty in capturing hazards related to ETCs (e.g., Colle et al., 2015; Catalano et al., 2019), emphasizing the importance of their process-level evaluation in weather and climate datasets.

Here we produce two-dimensional composites of several field associated with ETCs tracked in the first historical member of the Community Earth System Large Ensemble (Kay et al., 2015). ETCs over the northeastern United States were originally analyzed in this dataset in Zarzycki (2018). The years available for analysis in the historical simulations range from 1990-2015, inclusive. We also apply a pre-defined intensity threshold and spatially constrain ETCs to pass over the continental United States (CONUS) in order to demonstrate a regional analysis and highlight both filtering and compositing capabilities of TE.

3.4.1 Step 1: Generate trajectories

To begin, cyclonic storm trajectories are identified using DetectNodes by following sea level pressure (here, PSL) minima in 6-hourly data:

```
DetectNodes --in_data_list B20TRC5CNBDRD.001.PS_list.txt --out cyclone_candidates
  --closedcontourcmd "PSL,200.0,6.0,0" --mergedist 6.0
  --searchbymin "PSL" --outputcmd "PSL,min,0"
```

Our criteria for cyclonic storms is that the minimum pressure must be enclosed by a closed contour of 200 Pa within 6.0° of cyclone center. This minimum pressure location defines the cyclone center. Candidates within 6.0° of one another are merged, with the lower pressure taking precedence. Outputs from DetectNodes are then concatenated into a single candidate list, and StitchNodes is run to track these features in time:

```
StitchNodes --in_fmt "lon,lat,slp" --in_list candidate_list.txt --out etc-all-traj.txt
```

https://doi.org/10.5194/gmd-2020-303
Preprint. Discussion started: 20 January 2021


Geoscientific Model Development Discussions

```
  --range 6.0 --mintime 60h --maxgap 18h --min_endpoint_dist 12.0
  --threshold "lat,>,24,1;lon,>,234,1;lat,<,52,1;lon,<,294,1"
```

Here the StitchNodes thresholds require that storms persist for at least 60 hours, with a maximum gap (time between sequential detections satisfying the DetectNodes criteria) of at most 18 hours. Further, at least one point must pass through a geographic region (representing CONUS) bounded by 24°N and 52°N latitude and 234°E and 294°E longitude. We also require ETCs move at least 12° GCD from the start to the end of the trajectory, as specified by the `min_endpoint_dist` argument, in order to eliminate stationary features (e.g., the Icelandic Low) and spurious shallow lows generated over regions of high topography.

Note that while the algorithm is highly similar to that published in Zarzycki (2018), other ETC detection algorithms analogous to those published in the Intercomparison of Mid Latitude Storm Diagnostics (IMILAST, Neu et al. (2013)) can be configured using TE's command line options. Also, while a more complex algorithm could help eliminate cyclones that are tropical in nature, one is not applied here due to the relatively low resolution of CESM LENS. These coarser grid spacings are generally insufficient to resolve TCs (Walsh et al., 2015), although higher resolution evaluations of ETCs may require additional exclusionary thresholds to minimize their inclusion in storm track datasets if desired.

3.4.2 Step 2: NodeFileFilter and NodeFileEditor

To extract spatial information associated with ETCs we first filter a spatiotemporally continuous gridded dataset using NodeFileFilter:

```
NodeFileFilter --in_nodefile etc-all-traj.txt --in_fmt "lon,lat,slp"
  --in_data_list B20TRC5CNBDRD.001.PRECT_list.txt --out_data_list B20TRC5CNBDRD.001.PRECT_FI
  --var "PRECT" --bydist 25.0 --maskvar "mask"
```

Corresponding precipitation rate outputs from the same ensemble member are masked within 25° GCD of a storm center tracked in Step 1. Here, all precipitation associated with the cyclone is retained while all precipitation not within 25° of a storm is set to zero. A binary variable named 'mask' (as specified by argument `maskvar`) is also included to the filtered files for reference and can be used for offline masking and visualization.

Finally, all ETCs tracked in Step 1 are passed into NodeFileEditor, where a new trajectory file specified by argument `out_nodefile` is generated with storms only possessing intensities of 990 hPa or lower:

```
NodeFileEditor --in_nodefile etc-all-traj.txt
  --in_data_list B20TRC5CNBDRD.001.PRECT_list.txt
  --in_fmt "lon,lat,slp" --out_fmt "lon,lat,slp"
  --out_nodefile etc-strong-traj.txt
  --colfilter "slp,<=,99000."
```

Figure 4 shows the annual track density of all ETCs tracked in Step 1 (left) and the same plot but with only the subset of ETCs stronger than 990 hPa included (right). These results match those of other ETC trackers depicted in Neu et al. (2013).

https://doi.org/10.5194/gmd-2020-303
Preprint. Discussion started: 20 January 2021

Geoscientific Model Development Discussions

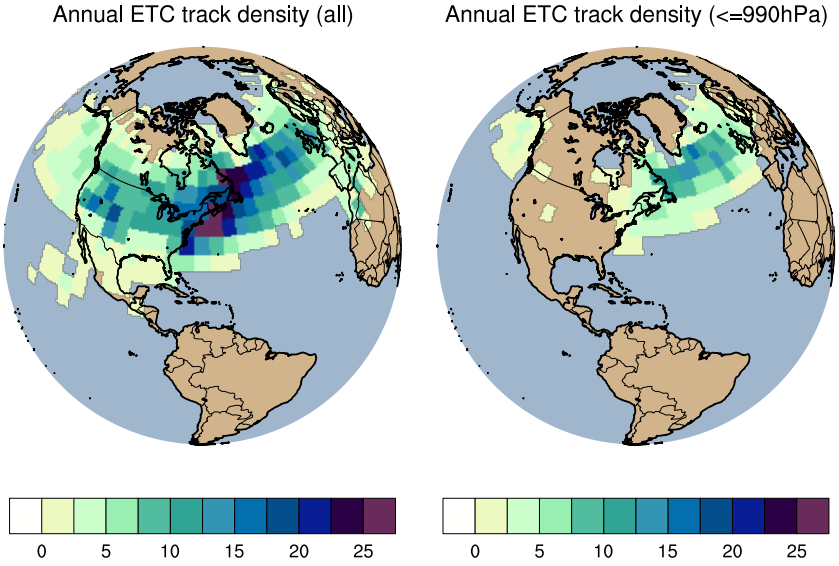

Figure 4. Track density maps for all CONUS ETCs tracked in the first historical member of CESM LENS (left) and only ETCs with simulated SLP less than or equal to 990 hPa. Units are number of six-hourly ETC occurrences per 5°x5° grid box per year.

3.4.3 Step 3: NodeFileCompose

As a last step, storm-centered composites are generated using the command:

```
NodeFileCompose --in_nodefile etc-strong-traj.txt --in_fmt "lon,lat,slp"
  --in_data_list B20TRC5CNBDRD.001.PRECT_FILT_list.txt --out_data "composite_PRECT.nc"
  --var "PRECT" --max_time_delta "2h" --op "mean" --dx 1.0 --resx 80
```

Here, only ETCs filtered above to have central SLP values below 990 hPa are composited. Although we can composite any 2D field, here we apply the compositing tool to precipitation filtered by NodeFileFilter. The argument `max_time_delta` indicates that the data slice nearest in time to the tracked feature (within 2 hours) should be composited – this is useful when the discrete times from data and features are not exactly aligned. The arithmetic mean is calculated centered on the storm location (see section 2.4). The resulting stereographic composite has grid spacing 1.0° and resolution 80x80.

3.4.4 Composited ETC fields

Figure 5 shows the composited precipitation rate field (`PRECT`), along with analogously calculated composites of 2-meter temperature (`TREFHT`) and specific humidity (`QREFHT`). Total precipitation is maximized near the storm center. Further, strong advection of warm, moist, equatorward air wrapping cyclonically around the storm center is seen in the near-surface temperature and moisture fields. This demonstrates that the heaviest ETC precipitation is associated with the warm conveyor belt, as previously shown in other hand-compositing studies (e.g., Field and Wood, 2007).

https://doi.org/10.5194/gmd-2020-303
Preprint. Discussion started: 20 January 2021

Geoscientific Model Development Discussions

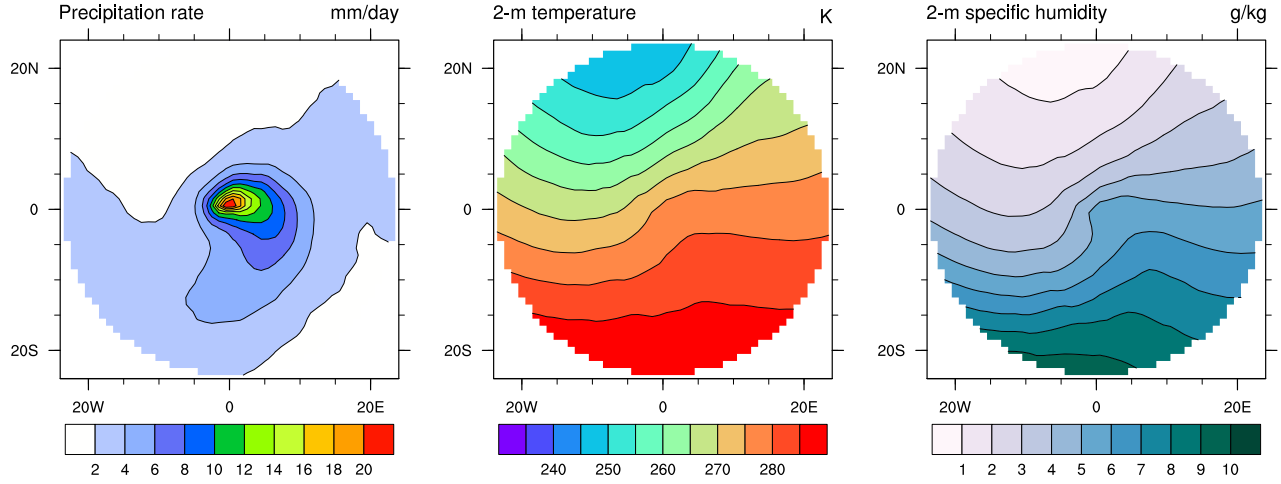

Figure 5. Composites of meteorological quantities centered on ETC storm center of all filtered storms with SLP less than or equal to 990 hPa in the first CESM-LENS historical member. From left to right are precipitation rate (mm day^{-1}), 2-meter temperature (K) and specific humidity (g kg^{-1}). 11,164 data points are included in each composite.

3.5 Atmospheric Rivers

Atmospheric rivers (ARs) are thin and long filamentary structures characterized by high integrated vapor transport (Payne et al., 2020). As claimed in Zhu and Newell (1998), ARs are responsible for approximately 90% of poleward vapor transport. In this section we identify ARs in ERA5 reanalysis using the Tempest AR detection algorithm (Shields et al., 2018; Rhoades et al., 2020b, a; McClenny et al., 2020), and extract the poleward vapor transport in order to verify this claim.

3.5.1 Step 1: DetectBlobs

ERA5 files containing vertically-integrated eastward vapor transport (VIWVE) and northward vapor transport (VIWVN) are first listed in `ERA5_IVT_files.txt`. The Tempest AR detection algorithm detects ARs as ridges in the IVT field, where IVT is defined pointwise as

$$\mathtt{IVT} = \sqrt{\mathtt{VIWVE}^2 + \mathtt{VIWVN}^2}. \tag{1}$$

Ridge points are associated with high downward curvature, and identified as those points where the Laplacian of the IVT field is below a fixed threshold (here chosen to be -2×10^4 kg m^{-2}s^{-1}rad^{-2}). The ridge points are useful indicators of the presence of ARs because this threshold identifies either long and narrow features or localized maxima (which are subsequently filtered using a minimum area criteria). Here the Laplacian is calculated using 8 radial points at a distance of 10° GCD (as described in Appendix B); this large stencil on the Laplacian provides some smoothing of the field. Note that all field manipulation routines are handled by TE internally. The command line for this operation is as follows:

```
DetectBlobs --in_data_list ERA5_IVT_files.txt --out_list ERA5_AR_files.txt
```

https://doi.org/10.5194/gmd-2020-303
Preprint. Discussion started: 20 January 2021


Geoscientific Model Development Discussions

```
  --timefilter "6hr"
  --thresholdcmd "_LAPLACIAN{8,10}(_VECMAG(VIWVE,VIWVN)),<=,-20000,0"
  --minabslat 15 --geofiltercmd "area,>=,4e5km2"
```

The first three command line arguments simply refer to the list of input files, output files and specify that data should be downsampled to 6-hourly timesteps. The meat of the operation is specified via the `thresholdcmd` argument, which uses the gridded data processor kernel built into TE to internally process the eastward and northward components of the integrated vapor transport (`VIWVE` and `VIWVN`, respectively) during the tagging operation. Specifically, the operation specified here identifies candidate grid points using a threshold on the Laplacian of the IVT. This command first calculates IVT using the vector magnitude operator, then calculates the Laplacian of the resulting field. Only points whose Laplacian is less than the threshold are retained. The last two arguments are then used to isolate high-IVT features near the equator (imposing a minimum absolute latitude of each grid tagged grid point of 15°), and a minimum area per blob of $4 \times 10^5\,\mathrm{km}^2$. Such filtering criteria are typical for AR trackers (Shields et al., 2018).

3.5.2 Step 2: NodeFileFilter

Using the thresholds above, tropical cyclones are sometimes picked up as part of the detection procedure. Using the ERA5 TC tracks produced in section 3.2 we can filter out points within a prescribed distance of these objects. This functionality uses the NodeFileFilter executable as follows:

```
NodeFileFilter --in_nodefile ERA5_TC_tracks.txt --in_fmt "lon,lat,slp,wind,zs"
  --in_data_list ERA5_AR_files.txt --out_data_list ERA5_AR_NFF_files.txt
  --var "binary_tag" --bydist 8.0 --invert
```

Here the nodefile from ERA5 is specified by `in_nodefile` and `in_fmt`. The input list of AR blobfiles, specified with `in_data_list` is the same as the output from DetectBlobs. The filtered output files are written to the filelist specified by `out_data_list`. The last two arguments here are key to the filtering procedure, specifying that the mask should include all points except those within 8 degrees GCD of each nodal feature.

Figure 6 shows the ERA5 integrated vapor transport (IVT) field on 2019-02-25 18:00 UTC, along with the outlines of AR objects detected using TE. On this date, an AR event on this date was responsible for flooding in California's Russian River basin (seen here intersecting the US West Coast). Dashed lines in this plot show the footprint of Super Typhoon Wutip at (139.75E, 15N) and Tropical Cyclone Pola at (175.5W, 14S), both of which have been excluded from the AR mask. Notably, Pola does not appear in IBTrACS until 2019-02-26 06:00:00 UTC.

3.5.3 Step 3: Apply AR mask to VIWVN

To now investigate AR and non-AR poleward moisture transport, we apply the mask generated in Step 2 to the `VIWVN` field (northward vapor transport). Here we leverage the VariableProcessor executable, which allows us to apply TE's built-in oper-

https://doi.org/10.5194/gmd-2020-303
Preprint. Discussion started: 20 January 2021

Geoscientific Model Development Discussions
Open Access
EGU

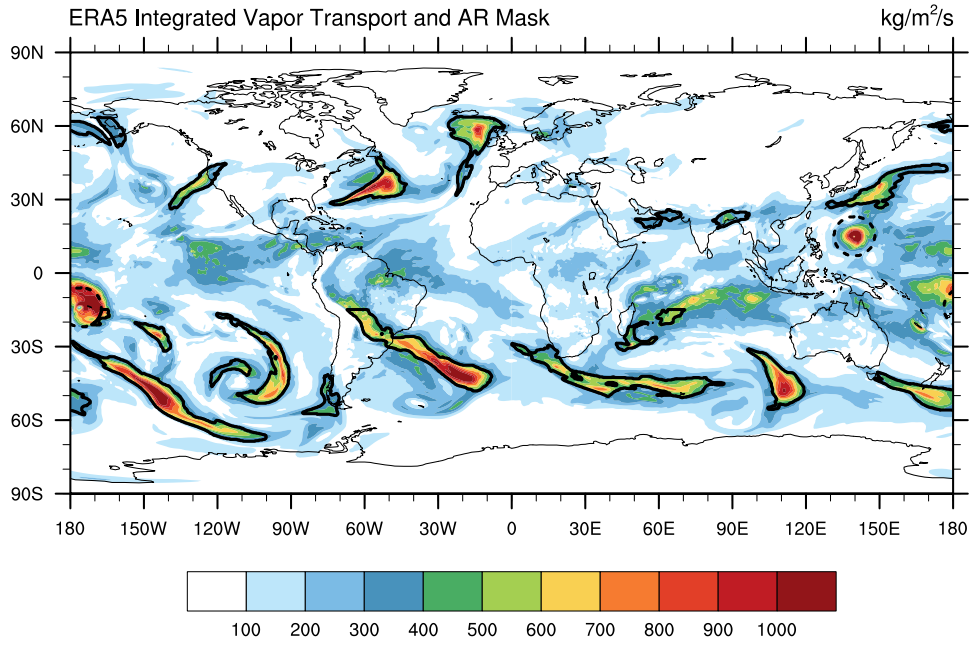

Figure 6. ERA5 integrated vapor transport (IVT) field with AR mask (black outlines) from 2019-02-25 18:00 UTC. Tropical cyclones that have been filtered from the AR mask are indicated with black dashed lines (8° radius GCD).

ations on a set of input files. Here the input file lis `ERA5_VPIN.txt` is the same as `ERA5_AR_NFF_files.txt`, except with the corresponding ERA5 VIWVN file appended to each line. To perform the processing we apply the command:

```
VariableProcessor --in_data_list ERA5_VPIN.txt --out_data_list ERA5_VPOUT.txt
  --timefilter "6hr"
  --var "_PROD(binary_tag,VIWVN));_PROD(_DIFF(1,binary_tag),VIWVN))"
  --varout "VIWVN_PW_AR,VIWVN_PW_NONAR"
```

The `var` argument here is specified to leverage TE's internal gridded variable processor. Since `binary_tag` only has value 0 or 1, the product of `VIWVN` and `binary_tag` will capture points within ARs, whereas the product of of `VIWVN` and `_DIFF(1,binary_tag)` will capture points not within ARs. These two variables are then written as `VIWVN_AR` and `VIWVN_NONAR` in the output file.

3.5.4 Poleward VIWVN from AR and non-AR points

Once AR and non-AR northward IVT have been calculated on a gridpoint level, the final processing step is handled outside of TE. To do so we take the time average and zonal average of the fields produced by VariableProcessor using NCO's robust record-averaging (`ncra`) and weighted averager (`ncwa`) operators. The zonal mean IVTn is then plotted in figure 7 for AR and non-AR points (top figure), along with the relative contribution to IVTn from ARs (bottom figure). The top figure here

https://doi.org/10.5194/gmd-2020-303
Preprint. Discussion started: 20 January 2021

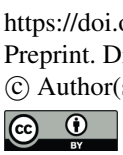

Geoscientific Model Development Discussions

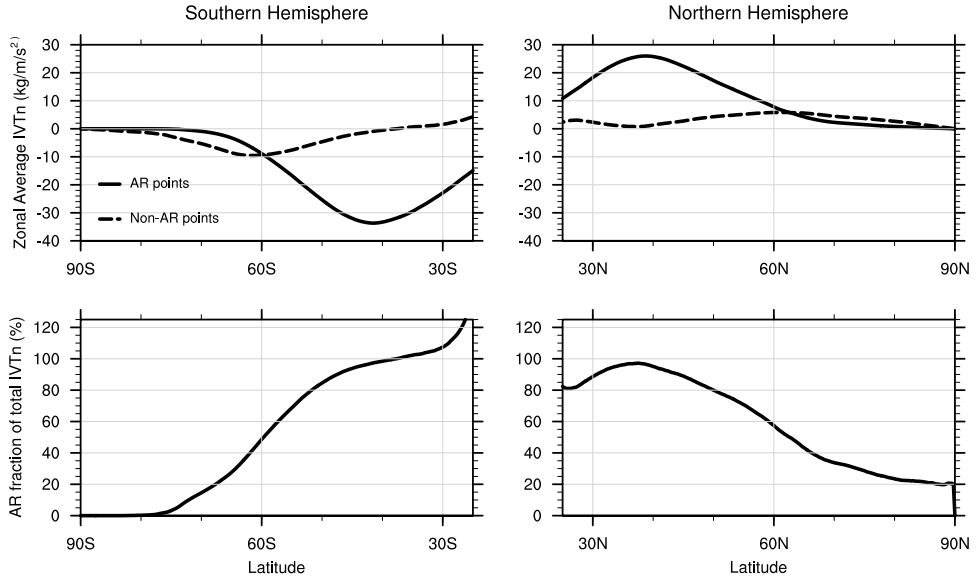

Figure 7. [top] Northward IVT (IVTn) from AR and non-AR grid points. [bottom] Fractional contribution to IVTn from AR points by latitude.

is complementary to Rutz et al. (2019) Figure 14 (middle), which was computed with 6-hourly MERRA2 data, and shows that the algorithm in this section exhibits results are consistent with other AR trackers. In the lower figure we see that the AR contribution to poleward transport is indeed close to 90% around 45N and 45S, although the contribution then decays precipitously at more poleward latitudes. Note, however, that this is in part because AR moisture transport is almost always poleward, whereas non-AR transport is a mix of both poleward and equatorward contributions.

3.6 Atmospheric Blocking

Our final example addresses the design of a tracker for detection of atmospheric blocking events, synoptic-scale weather phenomenon characterized by persistent obstruction of the normal westerly flow and associated with heat waves, cold spells, flooding and drought. In Pinheiro et al. (2019), several 2D algorithms were compared for the detection and characterization of blocking features. They find that the identification algorithm of Dole and Gordon (1983), which identifies blocks as anomalously high values of Z500, is fairly robust for global block detection and characterization.

3.6.1 Step 1: Generate Blocking Threshold

We describe here how to apply the `Z500` (geopotential height at 500hPa) anomaly algorithm globally to 3-hourly MERRA2 data (Gelaro et al., 2017). MERRA2 stores the 3D geopotential height variable in the `inst3_3d_asm_Np` dataset using variable name "H". For simplicity we assume that the input files contain a list of all files from this dataset from 1980/01/01-2020/06/30 (40.5 years). Within this dataset the 500hPa geopotential height variable can be specified by variable name

https://doi.org/10.5194/gmd-2020-303
Preprint. Discussion started: 20 January 2021

H(500hPa), where the vertical index is determined automatically by TE. The first step described in Pinheiro et al. (2019) is the construction of a Fourier-filtered long-term daily mean (LTDM) climatology of the Z500 field and its square. The Climatology executable is used in this step, and can be executed in parallel:

```
Climatology --in_data_list MERRA2_H_files.txt --out_data MERRA2_H_LTDM.nc
  --var "H(500hPa)" --period "daily" --type "mean" --missingdata
Climatology --in_data_list MERRA2_H_files.txt --out_data MERRA2_H2_LTDM.nc
  --var "H(500hPa)" --period "daily" --type "meansq" --missingdata
```

Here the missingdata argument is needed since the 500hPa pressure surface sometimes falls below the surface in the vicinity of the Himalayas, and consequently can cause problems if not employed. Note that, relevant to subsequent command lines, Climatology automatically prepends the descriptor "dailymean_" to the variable, so the final climatology is written to variable "dailymean_H".

We now calculate the standard deviation of the H(500hPa) field using the VariableProcessor:

```
VariableProcessor --in_data "MERRA2_H_LTDM.nc;MERRA2_H2_LTDM.nc"
  --out_data "MERRA2_H_mean_stddev.nc"
  --var "dailymean_H,_SQRT(_DIFF(dailymeansq_H,_POW(dailymean_H,2)))"
  --varout "dailymean_H,stddev_H"
```

We then apply a 4-mode Fourier filter to both the dailymean_H and stddev_H fields across the time dimension, and a 2-mode Fourier filter to the stddev_H field in the zonal direction:

```
FourierFilter --in_data MERRA2_H_mean_stddev.nc
  --out_data MERRA2_H_mean_stddev_timesmoothed.nc
  --var "dailymean_H,stddev_H" --dim "time" --modes 4
FourierFilter --in_data MERRA2_H_mean_stddev_timesmoothed.nc
  --out_data MERRA2_H_mean_stddev_smoothed.nc
  --var "stddev_H" --preserve "dailymean_H" --dim "lon" --modes 2
```

Finally the threshold is computed as $H500^* = \overline{H500} + \max\left(1.5 \times H500_{stddev}, 100\right)$ via the command line

```
VariableProcessor --in_data MERRA2_H_mean_stddev_smoothed.nc
  --out_data MERRA2_threshold_H_filtered.nc
  --var "_SUM(dailymean_H,_MAX(100.0,_PROD(1.5,stddev_H)))" --varout "threshold_H"
```

After performing these operations, a 365-day time series of the threshold field is obtained, plotted in Figure 8 on January 1st and July 1st. Note that this VariableProcessor operation could also have been performed using other climate data processing software, such as NetCDF operators or using a Python script; however, the parallelism built into TE allows for these computations to be performed rapidly on supercomputing systems.

https://doi.org/10.5194/gmd-2020-303
Preprint. Discussion started: 20 January 2021

Geoscientific Model Development Discussions

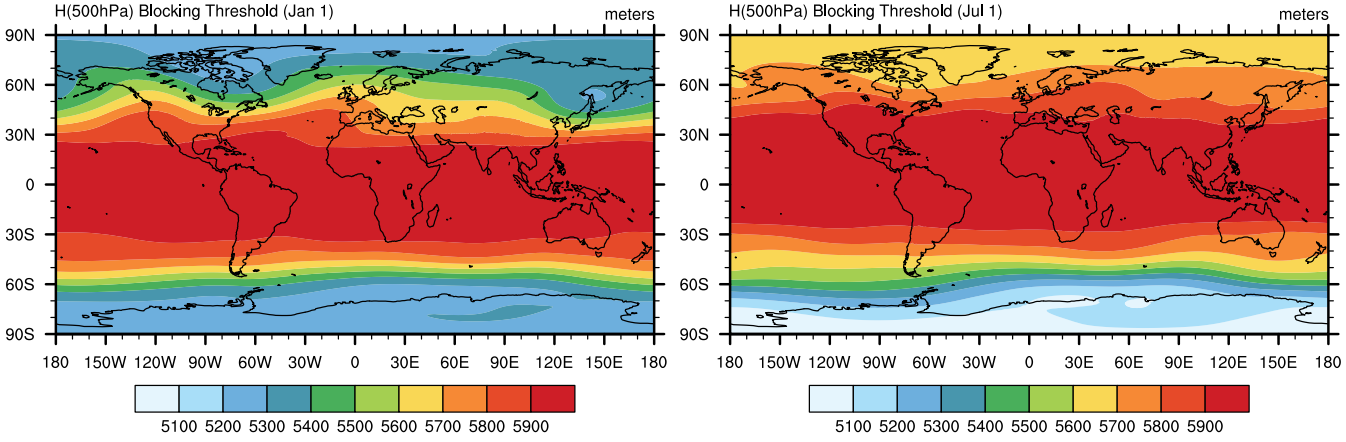

Figure 8. January 1st and July 1st MERRA2 blocking threshold generated with the command sequence in section 3.6.1.

3.6.2 Step 2: DetectBlobs

With the LTDM threshold in hand, we can now identify areal features that exceed this pointwise threshold. The newly generated LTDM threshold file is appended to each line of the input data list so it can be accessed by DetectBlobs. The output file list has the same number of lines as this input list, but points to the output files that will contain the binary tags for tagged points.

```
DetectBlobs
  --in_data_list MERRA2_DB_files.txt --out_list MERRA2_blocktag_files.txt
  --thresholdcmd "_DIFF(H(500hPa),threshold_H),>=,0,0"
  --minabslat 25  --maxabslat 75 --geofiltercmd "area,>,1e6km2" --tagvar "block_tag"
```

This command specifies points where 500 hPa geopotential height equals or exceeds the threshold are tagged as candidate blob points. We further remove candidate points equatorward of 25° N/S and poleward of 75° N/S and only retain contiguous regions whose are is at least $10^6 km^2$.

3.6.3 Step 3: StitchBlobs

The last step in block detection is to stitch together blobs from each timeslice to enable tracking of blobs in space and time. The StitchBlobs algorithm is described in detail in section 2.6. Here we use the command line:

```
StitchBlobs
  --in_list MERRA2_blocktag_files.txt --out_list MERRA2_blockid_files.txt
  --var "block_tag" --mintime "5d" --min_overlap_prev 20 --flatten
```

The criteria here require that blobs exist for at least 5 days continuously, and that blobs are considered to be connected in time only when 20% of the area of the blocked object at the previous time step is covered by the new blob (specified

https://doi.org/10.5194/gmd-2020-303
Preprint. Discussion started: 20 January 2021

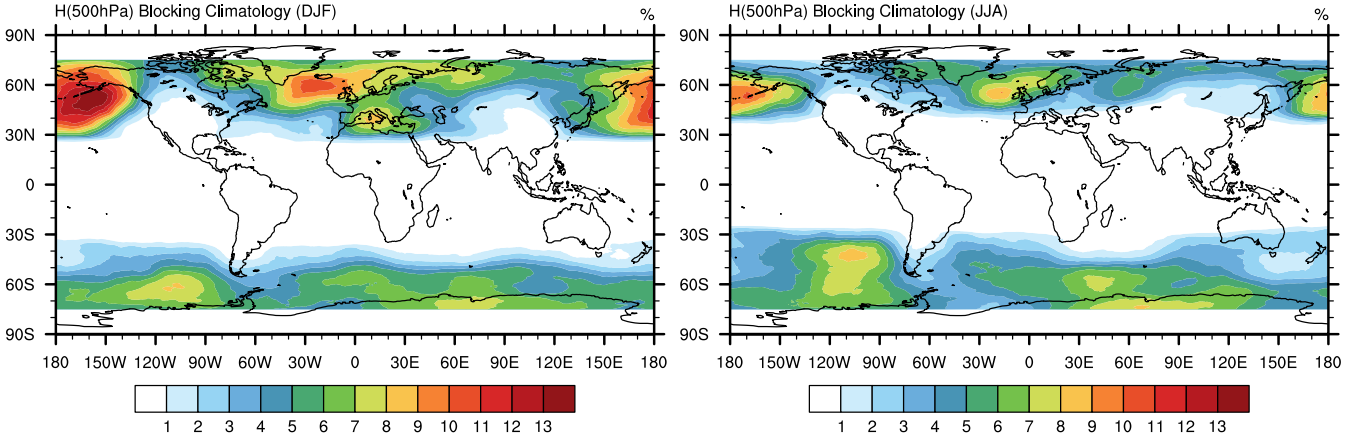

Figure 9. Percentage occurrence of blocking during (left) boreal winter and (right) boreal summer.

by `min_overlap_prev`). The `flatten` argument indicates that only binary occurrence of a feature (0 or 1) should be recorded after stitching. If this command was not specified then each object would be assigned a unique global integer identifier, as described in section 2.6.

3.6.4 Blocking climatology

The blocking data is then post-processed to build a seasonal climatology of blocking features. Since the presence of blocking is given with a binary indicator, this command is in effect calculating the fraction of timesteps where blocking occurs:

```
Climatology --in_data_list MERRA2_blockid_files.txt
  --out_data MERRA2_blocking_climo.nc --var "object_id" --period "seasonal"
```

The resulting blocking climatology in the boreal winter (December-January-February) and boreal summer (June-July-August) is depicted in Figure 9. The results are generally in agreement with the climatology of Pinheiro et al. (2019), and show substantial wintertime blocking in the North Atlantic and Pacific. A snapshot of blocked regions on 2013-12-07 6Z is further depicted in Figure 10 (black outlines). The blocking feature present in the Northern Pacific at the time was associated with anomalous dry conditions in California and anomalous warmth in Alaska.

4 Conclusions

Automated feature tracking capabilities have been frequently and successfully employed throughout the literature to evaluate regional and global models, investigate the drivers and environments of extreme weather events, and understand future change in the statistics of atmospheric features. Feature trackers further provide an important mechanism for extracting relevant information from large climate datasets, including reanalysis and observational datasets, and climate model simulations. This is particularly important as the stakeholder needs for climate data associated with societally relevant impacts grow larger.

https://doi.org/10.5194/gmd-2020-303
Preprint. Discussion started: 20 January 2021

Geoscientific Model Development Discussions

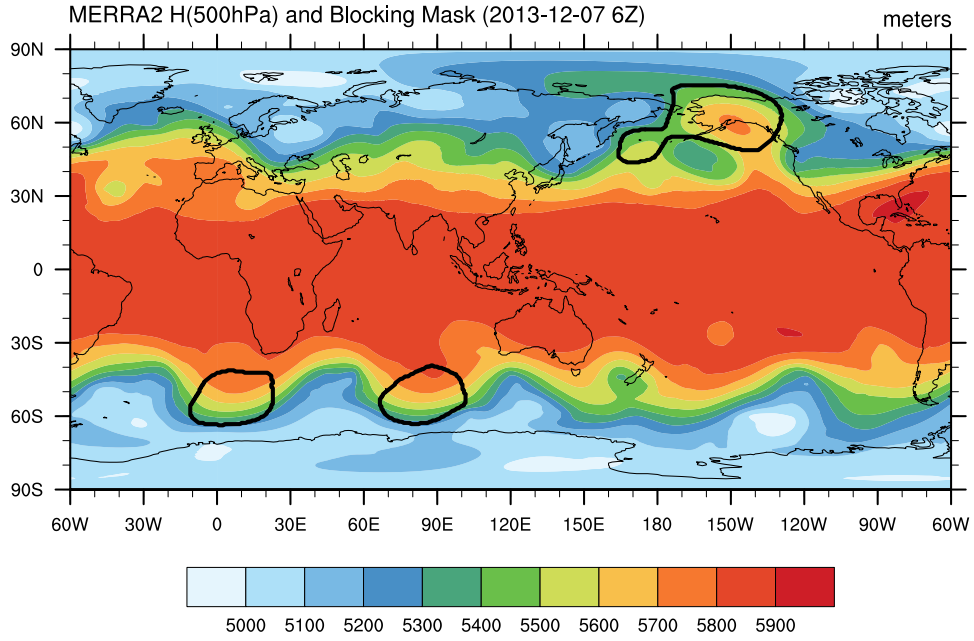

Figure 10. A snapshot of blocked regions in MERRA2 data detected on 2013-12-07 6Z (the three black outlines) atop the H(500hPa) field at this time.

As there are significant overlaps across the core functionality of these trackers, there is a clear added benefit to developing these kernels within a single framework. TempestExtremes (TE) is one such framework, with generalized kernels for identifying, characterizing, and analyzing both nodal and areal features. Although initially focused on tropical and extratropical cyclones (Ullrich and Zarzycki, 2017), TE has since added substantial functionality for areal feature tracking, characterizing and compositing features, and more dataset-agnostic command line arguments. TE has further continued to remain focused on high-throughput data processing, including continued MPI support for core executables. Such a framework has clear scientific relevance, enabling the development of feature catalogues, and addressing questions related to specific features (including those features commonly associated with extreme weather). As TE further exposes all tuning parameters on the command line, it allows users to easily investigate sensitivities of the tracker, or optimize the tracker for detecting particular features.

In this paper we have described some of the newer kernels exposed by TE, and shown how these kernels can be composited to build robust tracking algorithms for many consequential atmospheric features. The tracking capability enables the probing of deeper scientific questions related to individual features. To demonstrate this functionality, TE was employed in section 3.3 for tracking of tropical cyclones (TCs) and calculated the fractional contribution of TC precipitation to total precipitation in each region. Using TE we showed that TCs contribute to 20-40% of total precipitation in the tropical regions of the Pacific and South Indian Ocean in both satellite observations and ERA5 reanalysis. Ultimately, with the suite of trackers available in TE in hand, a global climatology can be constructed that attributes total precipitation to features. In section 3.4, an analysis of the composited characters of extratropical cyclones in the CESM large ensemble was performed to understand climatological

https://doi.org/10.5194/gmd-2020-303
Preprint. Discussion started: 20 January 2021

Geoscientific Model Development Discussions

track density and meteorological fields, enabling evaluation of model performance and better communication of the relevant underlying processes. In section 3.5, a novel atmospheric river detection algorithm was developed using TE and validated results related to meridional moisture transport put forward in Zhu and Newell (1998). Finally, in section 3.6, TE was used to construct a seasonal climatology of atmospheric blocking. Notably, the data reductions demonstrated in these sections enable feature-specific and process-oriented metrics and diagnostics that would streamline model evaluation.

It is expected that TE will continue to evolve to meet the needs of the scientific community. New kernels are already being investigated that encompass functionality present in other standalone trackers (Parfitt et al., 2017; Feng et al., 2018; Heikenfeld et al., 2019). It will further continue to maximize its robustness across datasets, so ensuring the framework is useful for standalone users and operational modeling centers, or for comparative analysis across reanalysis products, multi-model ensembles (Eyring et al., 2016) and single model ensembles (Kay et al., 2015). Finally, new capabilities to perform direct evaluation of simulation products in TE are now being developed, using the characteristics of tracked features as evaluation metrics.

Code availability. The TempestExtremes v2.1 release is available from ZENODO at https://dx.doi.org/10.5281/zenodo.4385656. The GitHub repository used for ongoing code development is available at https://github.com/ClimateGlobalChange/tempestextremes.

Appendix A: Stereographic Projection

The stereographic projection is used in the construction of composites using NodeFileFilter. The equations used for projection are provided here for reference.

The forward stereographic projection around a central point (λ_0, ϕ_0) is given by:

$$K = [1 + \sin\phi \sin\phi_0 + \cos\phi \cos\phi_0 \cos(\lambda - \lambda_0)]^{-1} \tag{A1}$$

$$X(\lambda, \phi; \lambda_0, \phi_0) = K \cos\phi \sin(\lambda - \lambda_0) \tag{A2}$$

$$Y(\lambda, \phi; \lambda_0, \phi_0) = K [\cos\phi_0 \sin\phi - \sin\phi_0 \cos\phi \cos(\lambda - \lambda_0)] \tag{A3}$$

The inverse projection is given by:

$$\rho = \sqrt{X^2 + Y^2}, \tag{A4}$$

$$c = 2 \arctan(\rho/2), \tag{A5}$$

$$\phi(X, Y; \lambda_0, \phi_0) = \begin{cases} \phi_0, & \text{if } \rho = 0, \\ \arcsin[\cos c \sin\phi_0 + (Y/\rho) \sin c \cos\phi_0], & \text{otherwise.} \end{cases} \tag{A6}$$

$$\lambda(X, Y; \lambda_0, \phi_0) = \begin{cases} \lambda_0, & \text{if } \rho = 0, \\ \lambda_0 + \arctan 2[X \sin c, \rho \cos\phi_0 \cos c - Y \sin\phi_0 \sin c], & \text{otherwise.} \end{cases} \tag{A7}$$

https://doi.org/10.5194/gmd-2020-303
Preprint. Discussion started: 20 January 2021

Geoscientific Model Development Discussions

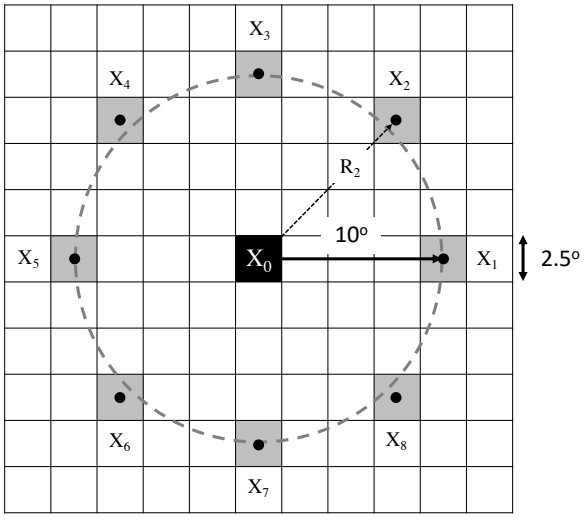

Figure B1. For a uniform (stereographic) grid with grid spacing of 2.5° GCD, an illustration of the grid points used in the calculation of the Laplacian with 8 radial points and radius 10° GCD. This operator is constructed in TE using notation `_LAPLACIAN{8,10}`. The central grid point is shaded black, and the modified centroids are shaded in gray.

Appendix B: Laplacian Operator

The stereographic discrete pointwise Laplacian operator defined in TE is constructed in a grid-independent manner using a discrete radial formulation. To begin, a set of N initial sample points are generated using a ring of radius R degrees around each grid point $\mathbf{X}_0$. Using a kd-tree-based implementation, the nearest grid points to each initial sample point are then selected to give a set of adjusted grid points $\mathbf{X}_n$ with $n = 1, \ldots, N$. For each of the initial sample points we then define the distance D_n by the great-circle distance between grid point X_0 and X_n. The averaged Laplacian over a disc of radius $R/2$ is then computed discretely using the divergence theorem on the stereographic plane and a centered difference approximation for the radial derivative:

$$\frac{1}{\pi(R/2)^2}\int \nabla^2 q dA = \frac{4}{\pi R^2}\oint \nabla q \cdot dS \approx \frac{4}{\pi R^2}\sum_{n=0}^{N-1}\left(\frac{q_n - q_0}{D_n}\right)\left(\frac{\pi R}{N}\right) = \frac{4}{NR}\sum_{n=0}^{N-1}\frac{q_n - q_0}{D_n} \tag{B1}$$

where q_n denotes the value of the field at X_n.

Author contributions. PAU wrote the software package with input from all involved authors and others in the community. CZ and KR advised on the algorithms for tracking tropical cyclones and extratropical cyclones. CZ further authored the extratropical cyclone section of the paper. EM advised on and tuned the algorithm for detecting and characterizing atmospheric rivers. MP developed the algorithm for detecting and characterizing atmospheric blocks. AS wrote the section on contributions of precipitation from tropical cyclones.

https://doi.org/10.5194/gmd-2020-303
Preprint. Discussion started: 20 January 2021


Geoscientific Model Development Discussions

Competing interests. The authors declare that they have no competing interests.

Acknowledgements. The authors would like to acknowledge the feedback and bug reports from our many users, particularly Alan Rhoades, Karthik Belaguru, Vishnu Sasidharan Nair, Erica Bower, and Yumin Moon. This work has been supported by Department of Energy Office of Science award number DE-SC0016605, "A Framework for Improving Analysis and Modeling of Earth System and Intersectoral Dynamics at Regional Scales (HyperFACETS)," NASA award NNX16AG62G "TempestExtremes: Indicators of change in the characteristics of extreme weather," NASA award 80NSSC19K0717 "Quantifying the link between organized convection and extreme precipitation," and NOAA MAPP award NA19OAR4310288 "Future changes in the frequency of winter snowstorms and their impact on snowfall and snow water equivalent." This project is also supported by the National Institute of Food and Agriculture, U.S. Department of Agriculture, hatch project under California Agricultural Experiment Station project accession no. 1016611. This research used resources of the National Energy Research Scientific Computing Center, a DOE Office of Science User Facility supported by the Office of Science of the U.S. Department of Energy under Contract No. DE-AC02-05CH11231.

https://doi.org/10.5194/gmd-2020-303
Preprint. Discussion started: 20 January 2021

References

Atkinson, G. D. and Holliday, C. R.: Tropical cyclone minimum sea level pressure/maximum sustained wind relationship for the Western North Pacific, Monthly Weather Review, 105, 421–427, https://doi.org/10.1175/1520-0493(1977)105<0421:TCMSLP>2.0.CO;2, 1977.

Balaguru, K., Leung, L. R., Van Roekel, L. P., Golaz, J.-C., Ullrich, P. A., Caldwell, P. M., Hagos, S. M., Harrop, B. E., and Mametjanov, A.: Characterizing Tropical Cyclones in the Energy Exascale Earth System Model Version 1, Journal of Advances in Modeling Earth Systems, 12, e2019MS002 024, 2020.

Bell, G. D., Halpert, M. S., Schnell, R. C., Higgins, R. W., Lawrimore, J., Kousky, V. E., Tinker, R., Thiaw, W., Chelliah, M., and Artusa, A.: Climate Assessment for 1999, Bulletin of the American Meteorological Society, 81, S1–S50, https://doi.org/10.1175/1520-0477(2000)81[s1:CAF]2.0.CO;2, 2000.

Camargo, S. J., Giulivi, C. F., Sobel, A. H., Wing, A. A., Kim, D., Moon, Y., Strong, J. D., Del Genio, A. D., Kelley, M., Murakami, H., Reed, K., Scoccimarro, E., Vecchi, G., Wehner, M., Zarzycki, C., and Zhao, M.: Characteristics of model tropical cyclone climatology and the large-scale environment, Journal of Climate, 33, 4463–4487, 2020.

Catalano, A. J., Broccoli, A. J., Kapnick, S. B., and Janoski, T. P.: High-Impact Extratropical Cyclones along the Northeast Coast of the United States in a Long Coupled Climate Model Simulation, Journal of Climate, 32, 2131–2143, https://doi.org/10.1175/JCLI-D-18-0376.1, 2019.

Chavas, D. R. and Reed, K. A.: Dynamical aquaplanet experiments with uniform thermal forcing: System dynamics and implications for tropical cyclone genesis and size, Journal of the Atmospheric Sciences, 76, 2257–2274, 2019.

Chavas, D. R., Reed, K. A., and Knaff, J. A.: Physical understanding of the tropical cyclone wind-pressure relationship, Nature Communications, 8, 1–11, https://doi.org/10.1038/s41467-017-01546-9, 2017.

Clark, A. J., Bullock, R. G., Jensen, T. L., Xue, M., and Kong, F.: Application of object-based time-domain diagnostics for tracking precipitation systems in convection-allowing models, Weather and Forecasting, 29, 517–542, 2014.

Colle, B. A., Booth, J. F., and Chang, E. K. M.: A Review of Historical and Future Changes of Extratropical Cyclones and Associated Impacts Along the US East Coast, Current Climate Change Reports, 1, 125–143, https://doi.org/10.1007/s40641-015-0013-7, 2015.

Dacre, H.: A review of extratropical cyclones: Observations and conceptual models over the past 100 years, Weather, 75, 4–7, https://doi.org/10.1002/wea.3653, https://rmets.onlinelibrary.wiley.com/doi/abs/10.1002/wea.3653, 2020.

Davini, P. and D'Andrea, F.: Northern Hemisphere atmospheric blocking representation in global climate models: Twenty years of improvements?, Journal of Climate, 29, 8823–8840, 2016.

Dean, J. and Ghemawat, S.: MapReduce: simplified data processing on large clusters, Communications of the ACM, 51, 107–113, 2008.

Di Luca, A., Evans, J. P., Pepler, A., Alexander, L., and Argüeso, D.: Resolution sensitivity of cyclone climatology over eastern Australia using six reanalysis products, Journal of Climate, 28, 9530–9549, 2015.

Dole, R. M. and Gordon, N. D.: Persistent anomalies of the extratropical Northern Hemisphere wintertime circulation: Geographical distribution and regional persistence characteristics, Monthly Weather Review, 111, 1567–1586, 1983.

Emanuel, K.: Increasing destructiveness of tropical cyclones over the past 30 years, Nature, 436, 686–688, 2005.

European Centre for Medium-Range Weather Forecasts: ERA5 Reanalysis (0.25 Degree Latitude-Longitude Grid), in: Research Data Archive at the National Center for Atmospheric Research, Computational and Information Systems Laboratory, National Center for Atmospheric Research (NCAR), https://doi.org/10.5065/BH6N-5N20, accessed 06 18 2020, 2019.

https://doi.org/10.5194/gmd-2020-303
Preprint. Discussion started: 20 January 2021

Eyring, V., Bony, S., Meehl, G. A., Senior, C. A., Stevens, B., Stouffer, R. J., and Taylor, K. E.: Overview of the Coupled Model Intercomparison Project Phase 6 (CMIP6) experimental design and organization, Geoscientific Model Development, 9, 1937–1958, 2016.

Feng, Z., Leung, L. R., Houze Jr, R. A., Hagos, S., Hardin, J., Yang, Q., Han, B., and Fan, J.: Structure and evolution of mesoscale convective systems: Sensitivity to cloud microphysics in convection-permitting simulations over the United States, Journal of Advances in Modeling Earth Systems, 10, 1470–1494, 2018.

Field, P. R. and Wood, R.: Precipitation and cloud structure in midlatitude cyclones, Journal of Climate, 20, 233–254, https://doi.org/10.1175/JCLI3998.1, https://doi.org/10.1175/JCLI3998.1, 2007.

Gelaro, R., McCarty, W., Suárez, M. J., Todling, R., Molod, A., Takacs, L., Randles, C. A., Darmenov, A., Bosilovich, M. G., Reichle, R., Wargan, K., Coy, L., Cullather, R., Draper, C., Akella, S., Buchard, V., Conaty, A., da Silva, A. M., Gu, W., Kim, G.-K., Koster, R., Lucchesi, R., Merkova, D., Nielsen, J. E., Partyka, G., Pawson, S., Putman, W., Rienecker, M., Schubert, S. D., Sienkiewicz, M., and Zhao, B.: The Modern-Era Retrospective Analysis for Research and Applications, version 2 (MERRA-2), Journal of Climate, 30, 5419–5454, 2017.

Grotjahn, R., Black, R., Leung, R., Wehner, M. F., Barlow, M., Bosilovich, M., Gershunov, A., Gutowski, W. J., Gyakum, J. R., Katz, R. W., Lee, Y.-Y., Lim, Y.-K., and Prabhat: North American extreme temperature events and related large scale meteorological patterns: A review of statistical methods, dynamics, modeling, and trends, Climate Dynamics, 46, 1151–1184, 2016.

Haarsma, R. J., Roberts, M. J., Vidale, P. L., Senior, C. A., Bellucci, A., Bao, Q., Chang, P., Corti, S., Fučkar, N. S., Guemas, V., von Hardenberg, J., Hazeleger, W., Kodama, C., Koenigk, T., Leung, L. R., Lu, J., Luo, J.-J., Mao, J., Mizielinski, M. S., Mizuta, Ryo Nobre, P., Satoh, M., Scoccimarro, E., Semmler, T., Small, J., and von Storch, J.-S.: High resolution model intercomparison project (HighResMIP v1. 0) for CMIP6, Geoscientific Model Development, 9, 4185–4208, 2016.

Hart, R. E.: A cyclone phase space derived from thermal wind and thermal asymmetry, Monthly Weather Review, 131, 585–616, 2003.

Hassani, H., Huang, X., and Silva, E.: Big Data and climate change, Big Data and Cognitive Computing, 3, 12, 2019.

Heikenfeld, M., Marinescu, P. J., Christensen, M., Watson-Parris, D., Senf, F., Van Den Heever, S. C., and Stier, P.: tobac v1.2: Towards a flexible framework for tracking and analysis of clouds in diverse datasets, Geoscientific Model Development, 12, 4551–4570, 2019.

Hersbach, H., Bell, B., Berrisford, P., Hirahara, S., Horányi, A., Muñoz-Sabater, J., Nicolas, J., Peubey, C., Radu, R., Schepers, D., Simmons, A., Soci, C., Abdalla, S., Abellan, X., Balsamo, G., Bechtold, P., Biavati, G., Bidlot, J., Bonavita, M., Chiara, G. D., Dahlgren, P., Dee, D., Diamantakis, M., Dragani, R., Flemming, J., Forbes, R., Fuentes, M., Geer, A., Haimberger, L., Healy, S., Hogan, R. J., Hólm, E., Janisková, M., Keeley, S., Laloyaux, P., Lopez, P., Lupu, C., Radnoti, G., de Rosnay, P., Rozum, I., Vamborg, F., Villaume, S., and Thépaut, J.: The ERA5 global reanalysis, Quarterly Journal of the Royal Meteorological Society, 146, 1999–2049, 2020.

Hodges, K., Cobb, A., and Vidale, P. L.: How well are tropical cyclones represented in reanalysis datasets?, Journal of Climate, 30, 5243–5264, https://doi.org/10.1175/JCLI-D-16-0557.1, 2017.

Holland, G.: A revised hurricane pressure-wind model, Monthly Weather Review, 136, 3432–3445, https://doi.org/10.1175/2008MWR2395.1, 2008.

Hope, P., Keay, K., Pook, M., Catto, J., Simmonds, I., Mills, G., McIntosh, P., Risbey, J., and Berry, G.: A comparison of automated methods of front recognition for climate studies: A case study in southwest Western Australia, Monthly Weather Review, 142, 343–363, 2014.

Huffman, G. J., Bolvin, D. T., Nelkin, E. J., Wolff, D. B., Adler, R. F., Gu, G., Hong, Y., Bowman, K. P., and Stocker, E. F.: The TRMM Multisatellite Precipitation Analysis (TMPA): Quasi-global, multiyear, combined-sensor precipitation estimates at fine scales, Journal of Hydrometeorology, 8, 38–55, https://doi.org/10.1175/JHM560.1, 2007.

https://doi.org/10.5194/gmd-2020-303
Preprint. Discussion started: 20 January 2021

Hurley, J. V. and Boos, W. R.: A global climatology of monsoon low-pressure systems, Quarterly Journal of the Royal Meteorological Society, 141, 1049–1064, 2015.

Kay, J. E., Deser, C., Phillips, A., Mai, A., Hannay, C., Strand, G., Arblaster, J. M., Bates, S., Danabasoglu, G., Edwards, J., Holland, M., Kushner, P., Lamarque, J.-F., Lawrence, D., Lindsay, K., Middleton, A., Munoz, E., Neale, R., Oleson, K., Polvani, L., and Vertenstein, M.: The Community Earth System Model (CESM) large ensemble project: A community resource for studying climate change in the presence of internal climate variability, Bulletin of the American Meteorological Society, 96, 1333–1349, 2015.

Khouakhi, A., Villarini, G., and Vecchi, G. A.: Contribution of tropical cyclones to rainfall at the global scale, Journal of Climate, 30, 359–372, https://doi.org/10.1175/JCLI-D-16-0298.1, 2017.

Knaff, J. A. and Zehr, R. M.: Reexamination of tropical cyclone wind–pressure relationships, Weather and Forecasting, 22, 71–88, https://doi.org/10.1175/WAF965.1, 2007.

Knapp, K. R., Kruk, M. C., Levinson, D. H., Diamond, H. J., and Neumann, C. J.: The International Best Track Archive for Climate Stewardship (IBTrACS) unifying tropical cyclone data, Bulletin of the American Meteorological Society, 91, 363–376, 2010.

Li, F., Chavas, D. R., Reed, K. A., and Dawson II, D. T.: Climatology of severe local storm environments and synoptic-scale features over North America in ERA5 reanalysis and CAM6 simulation, Journal of Climate, 33, 8339–8365, https://doi.org/10.1175/JCLI-D-19-0986.1, 2020.

McClenny, E. E., Ullrich, P. A., and Grotjahn, R.: Sensitivity of atmospheric river vapor transport and precipitation to uniform sea-surface temperature increases, Journal of Geophysical Research: Atmospheres, 125, https://doi.org/10.1029/2020JD033421, e2020JD033421, 2020.

Michaelis, A. C. and Lackmann, G. M.: Climatological changes in the extratropical transition of tropical cyclones in high-resolution global simulations, Journal of Climate, 32, 8733–8753, 2019.

Moon, Y., Kim, D., Camargo, S. J., Wing, A. A., Sobel, A. H., Murakami, H., Reed, K. A., Scoccimarro, E., Vecchi, G. A., Wehner, M. F., Zarzycki, C. M., and Zhao, M.: Azimuthally averaged wind and thermodynamic structures of tropical cyclones in global climate models and their sensitivity to horizontal resolution, Journal of Climate, 33, 1575–1595, 2020.

Murakami, H.: Tropical cyclones in reanalysis data sets, Geophysical Research Letters, 41, 2133–2141, https://doi.org/10.1002/2014GL059519, 2014.

Murata, A., Sasaki, H., Kawase, H., and Nosaka, M.: The development of a resolution-independent tropical cyclone detection scheme for high-resolution climate model simulations, Journal of the Meteorological Society of Japan. Ser. II, 2019.

Neu, U., Akperov, M. G., Bellenbaum, N., Benestad, R., Blender, R., Caballero, R., Cocozza, A., Dacre, H. F., Feng, Y., Fraedrich, K., et al.: IMILAST: A community effort to intercompare extratropical cyclone detection and tracking algorithms, Bulletin of the American Meteorological Society, 94, 529–547, 2013.

Parfitt, R., Czaja, A., and Seo, H.: A simple diagnostic for the detection of atmospheric fronts, Geophysical Research Letters, 44, 4351–4358, 2017.

Patricola, C. M., O'Brien, J. P., Risser, M. D., Rhoades, A. M., O'Brien, T. A., Ullrich, P. A., Stone, D. A., and Collins, W. D.: Maximizing ENSO as a source of western US hydroclimate predictability, Climate Dynamics, 54, 351–372, 2020.

Payne, A. E., Demory, M.-E., Leung, L. R., Ramos, A. M., Shields, C. A., Rutz, J. J., Siler, N., Villarini, G., Hall, A., and Ralph, F. M.: Responses and impacts of atmospheric rivers to climate change, Nature Reviews Earth & Environment, pp. 1–15, 2020.

https://doi.org/10.5194/gmd-2020-303
Preprint. Discussion started: 20 January 2021

Pendergrass, A. G., Reed, K. A., and Medeiros, B.: The link between extreme precipitation and convective organization in a warming climate: Global radiative-convective equilibrium simulations, Geophysical Research Letters, 43, 11,445–11,452, https://doi.org/10.1002/2016GL071285, 2016.

Pinheiro, M., Ullrich, P., and Grotjahn, R.: Atmospheric blocking and intercomparison of objective detection methods: flow field characteristics, Climate dynamics, 53, 4189–4216, 2019.

Powell, M. D. and Reinhold, T. A.: Tropical cyclone destructive potential by integrated kinetic energy, Bulletin of the American Meteorological Society, 88, 513–526, 2007.

Prat, O. P. and Nelson, B. R.: Mapping the world's tropical cyclone rainfall contribution over land using the TRMM Multi-satellite Precipitation Analysis, Water Resources Research, 49, 7236–7254, https://doi.org/https://doi.org/10.1002/wrcr.20527, 2013.

Prein, A. F., Liu, C., Ikeda, K., Trier, S. B., Rasmussen, R. M., Holland, G. J., and Clark, M. P.: Increased rainfall volume from future convective storms in the US, Nature Climate Change, 7, 880–884, 2017.

Reed, K. A., Stansfield, A., Wehner, M., and Zarzycki, C.: Forecasted attribution of the human influence on Hurricane Florence, Science advances, 6, eaaw9253, 2020.

Rhoades, A., Jones, A., Srivastava, A., Huang, H., O'Brien, T., Patricola, C., Ullrich, P., Wehner, M., and Zhou, Y.: The shifting scales of Western US landfalling atmospheric rivers under climate change, Geophysical Research Letters, in press, 2020a.

Rhoades, A. M., Jones, A. D., O'Brien, T. A., O'Brien, J. P., Ullrich, P. A., and Zarzycki, C. M.: Influences of North Pacific Ocean domain extent on the Western US winter hydroclimatology in variable-resolution CESM, Journal of Geophysical Research: Atmospheres, 125, e2019JD031 977, 2020b.

Roberts, M. J., Camp, J., Seddon, J., Vidale, P. L., Hodges, K., Vannière, B., Mecking, J., Haarsma, R., Bellucci, A., Scoccimarro, E., Caron, L.-P., Chauvin, F., Terray, L., Valcke, S., Moine, M.-P., Putrasahan, D., Roberts, C., Senan, R., Zarzycki, C., Ullrich, P., Yamada, Y., Mizuta, R., Kodama, C., Fu, D., Zhang, Q., Danabasoglu, G., Rosenbloom, N., Wang, H., and Wu, L.: Projected future changes in tropical cyclones using the CMIP6 HighResMIP multimodel ensemble, Geophysical Research Letters, 47, e2020GL088 662, 2020a.

Roberts, M. J., Camp, J., Seddon, J., Vidale, P. L., Hodges, K., Vanniere, B., Mecking, J., Haarsma, R., Bellucci, A., Scoccimarro, E., Caron, L.-P., Chauvin, F., Terray, L., Valcke, S., Moine, M.-P., Putrasahan, D., Roberts, C., Senan, R., Zarzycki, C., Ullrich, P., Yamada, Y., Mizuta, R., Kodama, C., Fu, D., Zhang, Q., Danabasoglu, G., Rosenbloom, N., Wang, H., and Wu, L.: Impact of model resolution on tropical cyclone simulation using the HighResMIP–PRIMAVERA multimodel ensemble, Journal of Climate, 33, 2557–2583, 2020b.

Rutz, J. J., Shields, C. A., Lora, J. M., Payne, A. E., Guan, B., Ullrich, P., O'Brien, T., Leung, L. R., Ralph, F. M., Wehner, M., Brands, S., Collow, A., Goldenson, N., Gorodetskaya, I., Griffith, H., Kashinath, K., Kawzenuk, B., Krishnan, H., Kurlin, V., Lavers, D., Magnusdottir, G., Mahoney, K., McClenny, E., Muszynski, G., Nguyen, P. D., Prabhat, Qian, Y., Ramos, A. M., Sarangi, C., Sellars, S., Shulgina, T., Tome, R., Waliser, D., Walton, D., Wick, G., Wilson, A. M., and Viale, M.: The Atmospheric River Tracking Method Intercomparison Project (ARTMIP): Quantifying uncertainties in atmospheric river climatology, Journal of Geophysical Research: Atmospheres, 124, 13 777–13 802, 2019.

Schemm, S., Rudeva, I., and Simmonds, I.: Extratropical fronts in the lower troposphere–global perspectives obtained from two automated methods, Quarterly Journal of the Royal Meteorological Society, 141, 1686–1698, 2015.

Schenkel, B. A. and Hart, R. E.: An examination of tropical cyclone position, intensity, and intensity life cycle within atmospheric reanalysis datasets, Journal of Climate, 25, 3453–3475, https://doi.org/10.1175/2011JCLI4208.1, 2012.

Schenkel, B. A., Lin, N., Chavas, D., Oppenheimer, M., and Brammer, A.: Evaluating outer tropical cyclone size in reanalysis datasets using QuikSCAT data, Journal of Climate, 30, 8745–8762, 2017.

https://doi.org/10.5194/gmd-2020-303
Preprint. Discussion started: 20 January 2021

Scherrer, S. C., Croci-Maspoli, M., Schwierz, C., and Appenzeller, C.: Two-dimensional indices of atmospheric blocking and their statistical relationship with winter climate patterns in the Euro-Atlantic region, International Journal of Climatology: A Journal of the Royal Meteorological Society, 26, 233–249, 2006.

Schnase, J. L., Lee, T. J., Mattmann, C. A., Lynnes, C. S., Cinquini, L., Ramirez, P. M., Hart, A. F., Williams, D. N., Waliser, D., Rinsland, P., Webster, W. P., Duffy, D. Q., McInerney, M. A., Tamkin, G. S., Potter, G. L., and Carriere, L.: Big data challenges in climate science: Improving the next-generation cyberinfrastructure, IEEE geoscience and remote sensing magazine, 4, 10–22, 2016.

Schultz, D. M., Bosart, L. F., Colle, B. A., Davies, H. C., Dearden, C., Keyser, D., Martius, O., Roebber, P. J., Steenburgh, W. J., Volkert, H., and Winters, A. C.: Extratropical cyclones: A century of research on meteorology's centerpiece, Meteorological Monographs, 59, 16.1–16.56, https://doi.org/10.1175/AMSMONOGRAPHS-D-18-0015.1, 2019.

Shields, C. A., Rutz, J. J., Leung, L.-Y., Ralph, F. M., Wehner, M., Kawzenuk, B., Lora, J. M., McClenny, E., Osborne, T., Payne, A. E., Ullrich, P., Gershunov, A., Goldenson, N., Guan, B., Qian, Y., Ramos, A. M., Sarangi, C., Sellars, S., Gorodetskaya, I., Kashinath, K., Kurlin, V., Mahoney, K., Muszynski, G., Pierce, R., Subramanian, A. C., Tome, R., Waliser, D., Walton, D., Wick, G., Wilson, A., Lavers, D., Collow, A., Krishnan, H., Magnusdottir, G., and Nguyen, P.: Atmospheric river tracking method intercomparison project (ARTMIP): project goals and experimental design, Geoscientific Model Development (Online), 11, 2018.

Small, R. J., Msadek, R., Kwon, Y.-O., Booth, J. F., and Zarzycki, C.: Atmosphere surface storm track response to resolved ocean mesoscale in two sets of global climate model experiments, Climate Dynamics, 52, 2067–2089, 2019.

Stansfield, A. M., Reed, K. A., Zarzycki, C. M., Ullrich, P. A., and Chavas, D. R.: Assessing tropical cyclones' contribution to precipitation over the Eastern United States and sensitivity to the variable-resolution domain extent, Journal of Hydrometeorology, 21, 1425–1445, 2020.

Ullrich, P. A.: TempestExtremes User Guide, https://climate.ucdavis.edu/tempestextremes.php, 2020.

Ullrich, P. A. and Zarzycki, C. M.: TempestExtremes: A framework for scale-insensitive pointwise feature tracking on unstructured grids, Geoscientific Model Development, 10, 1069, 2017.

Vishnu, S., Boos, W., Ullrich, P., and O'Brien, T.: Assessing historical variability of South Asian monsoon lows and depressions with an optimized tracking algorithm, Journal of Geophysical Research: Atmospheres, p. e2020JD032977, 2020.

Walsh, K. J. E., Camargo, S. J., Vecchi, G. A., Daloz, A. S., Elsner, J., Emanuel, K., Horn, M., Lim, Y.-K., Roberts, M., Patricola, C., Scoccimarro, E., Sobel, A. H., Strazzo, S., Villarini, G., Wehner, M., Zhao, M., Kossin, J. P., LaRow, T., Oouchi, K., Schubert, S., Wang, H., Bacmeister, J., Chang, P., Chauvin, F., Jablonowski, C., Kumar, A., Murakami, H., Ose, T., Reed, K. A., Saravanan, R., Yamada, Y., Zarzycki, C. M., Vidale, P. L., Jonas, J. A., and Henderson, N.: Hurricanes and climate: The U.S. CLIVAR working group on hurricanes, Bulletin of the American Meteorological Society, 96, 997–1017, https://doi.org/10.1175/BAMS-D-13-00242.1, 2015.

Wing, A. A., Camargo, S. J., Sobel, A. H., Kim, D., Moon, Y., Murakami, H., Reed, K. A., Vecchi, G. A., Wehner, M. F., Zarzycki, C., et al.: Moist static energy budget analysis of tropical cyclone intensification in high-resolution climate models, Journal of Climate, 32, 6071–6095, 2019.

Zarzycki, C. M.: Tropical cyclone intensity errors associated with lack of two-way ocean coupling in high-resolution global simulations, Journal of Climate, 29, 8589–8610, 2016.

Zarzycki, C. M.: Projecting changes in societally impactful northeastern US snowstorms, Geophysical Research Letters, 45, 12–067, 2018.

Zarzycki, C. M. and Ullrich, P. A.: Assessing sensitivities in algorithmic detection of tropical cyclones in climate data, Geophysical Research Letters, 44, 1141–1149, 2017.

https://doi.org/10.5194/gmd-2020-303
Preprint. Discussion started: 20 January 2021

Zarzycki, C. M., Thatcher, D. R., and Jablonowski, C.: Objective tropical cyclone extratropical transition detection in high-resolution reanalysis and climate model data, Journal of Advances in Modeling Earth Systems, 9, 130–148, 2017.

Zarzycki, C. M., Reed, K. A., and Ullrich, P. A.: Metrics for evaluating tropical cyclones in climate data, Journal of Applied Meteorology and Climatology, revised.

Zender, C. S.: Analysis of self-describing gridded geoscience data with netCDF Operators (NCO), Environmental Modelling & Software, 23, 1338–1342, https://doi.org/10.1016/j.envsoft.2008.03.004, 2008.

Zhang, W., Hari, V., and Villarini, G.: Potential impacts of anthropogenic forcing on the frequency of tropical depressions in the North Indian Ocean in 2018, Journal of Marine Science and Engineering, 7, 436, 2019.

Zhang, W., Villarini, G., Scoccimarro, E., and Napolitano, F.: Examining the precipitation associated with Medicanes in the high-resolution ERA-5 reanalysis data, International Journal of Climatology, 2020.

Zhu, Y. and Newell, R. E.: A proposed algorithm for moisture fluxes from atmospheric rivers, Monthly Weather Review, 126, 725–735, 1998.